PART ONE

THE EFFECT OF A SIMPLE THROAT DISTORTION ON THE DOWNSTREAM FLOW IN A HYPERSONIC WIND TUNNEL NOZZLE

and

PART TWO

AN EXPERIMENTAL INVESTIGATION OF FLOW OVER SIMPLE BLUNT BODIES AT A NOMINAL MACH NUMBER OF 5.8

Thesis by

R. E. Oliver

In Partial Fulfillment of the Requirements

For the Degree of

Aeronautical Engineer

California Institute of Technology

Pasadena, California

1957

ACKNOWLEDGMENTS

The author wishes to express his appreciation for the many helpful suggestions and the guidance provided by Dr. C. B. Millikan, Dr. H. T. Nagamatsu, Prof. L. Lees, Mr. Toshi Kubota, and Mr. B. E. Cummings of GALCIT, and Dr. P. Wegener of the Jet Propulsion Laboratory.

These investigations were carried out under the sponsorship and with the financial support of the Office, Chief of Ordnance, and the Office of Ordnance Research, U. S. Army. The nozzle and test section used in the investigation of Part One were designed and built by the Jet Propulsion Laboratory staff, and the distorted throat configuration was proposed by Dr. Joseph Sternberg of the Ballistic Research Laboratory, Aberdeen Proving Grounds, Maryland.

The author wishes to thank Anne J. Graff for the final typing of this thesis.

ABSTRACT

PART ONE

An experimental investigation was conducted in the GALCIT 2 1/2 inch Supersonic Wind Tunnel to determine the effect of a known distortion of the throat section of a hypersonic nozzle on the flow in the region downstream from the throat. The flow in a nozzle with a rectangular throat section was compared with the flow in the same nozzle with the throat region distorted to produce a throat height which varied linearly across the throat section. The flow was investigated by means of Pitot pressure surveys in the horizontal plane of symmetry of the undistorted nozzle.

The magnitude of the effect produced by the throat distortion was observed to be approximately that predicted by one-dimensional isentropic flow relations. However, the sign of the effect was reversed in about the distance required for a curved Mach line starting at the throat to cross the channel.

PART TWO

An experimental investigation was conducted in Leg No. 1 of the GALCIT Hypersonic Wind Tunnel to determine flow characteristics for a series of blunt bodies at a nominal Mach number of 5.80

and free stream Reynolds numbers per inch of 2.4×10^5, 1.2×10^5, and 0.6×10^5. The scope of this investigation was to determine surface static pressure distributions and to obtain schlieren photographs showing the shock configurations. The seven bodies investigated were as follows: (1) 40° half-angle cone; (2) 40° half-angle cone with spherical nose; (3) hemisphere-cylinder; (4) cylinder transverse to the free stream flow; (5) flat-nosed cylinder with its major axis parallel to the free stream flow direction; (6) $10^\circ - 40^\circ$ half-angle double cone; and (7) $13^\circ - 30^\circ$ half-angle double cone. All tests were conducted in one-phase flow with a tunnel stagnation temperature of $225^\circ F$ and with models at zero angles of attack and yaw.

TABLE OF CONTENTS

LIST OF SYMBOLS

C_p = $\Delta p/q$ = pressure coefficient

γ ratio of specific heats of the fluid

D characteristic length used in defining Reynolds number

η angle between the free stream flow direction and the normal to the body surface element

θ central angle of a spherical or cylindrical body measured from the stagnation point

μ_∞ absolute viscosity of the fluid in the free stream

M_∞ free stream Mach number

p_∞ free stream static pressure

p_o reservoir or total pressure

p_o' total pressure downstream from a normal shock

p_s local static pressure

$\Delta p = p_s - p_\infty$

$q = \frac{1}{2} \rho_\infty U_\infty^2$ = dynamic pressure

ρ_∞ free stream mass density

ρ_2 mass density behind a normal shock

$R_e = \frac{\rho_\infty D U_\infty}{\mu_\infty}$ = free stream Reynolds number

U_∞ = free stream velocity

LIST OF FIGURES

LIST OF FIGURES (Cont'd.)

PART ONE

THE EFFECT OF A SIMPLE THROAT DISTORTION ON THE DOWNSTREAM FLOW IN A HYPERSONIC WIND TUNNEL NOZZLE

I. INTRODUCTION

Hypersonic wind tunnel nozzles are designed to operate at stagnation temperatures sufficiently high to prevent condensation of air in the test region. The required stagnation temperature increases rapidly with increasing test section Mach number. For example (assuming no super-saturation), for a test section Mach number of 6 and a reservoir pressure of 100 psia, the stagnation temperature must be at least 300°F, while for a test section Mach number of 9 and a reservoir pressure of 500 psia, the stagnation temperature must be at least 1,050°F. For high Mach number nozzles the high heat transfer rates in the throat region resulting from the high stagnation temperatures can obviously produce large thermal expansions or distortions of the nozzle material unless this region is either cooled or is made from a material with low thermal expansion properties. Either method of avoiding thermal distortions in the throat region presents a difficult design problem. The amount of throat distortion which can be tolerated is then of prime importance to the designer of hypersonic wind tunnel nozzles.

This investigation was undertaken to provide some quantitative information about the effect of a known throat distortion on the flow properties in the region downstream from the throat. The scope of the investigation was to determine the streamwise distance-history of the distortion effect in the horizontal plane of symmetry of the undistorted nozzle.

II. EXPERIMENTAL EQUIPMENT AND PROCEDURE

A. Description of the Wind Tunnel

The experimental investigation was carried out in the GALCIT 2 1/2 x 3 inch Supersonic Wind Tunnel. This facility is described in Reference 1. Both the Supersonic and Hypersonic compressor plants were used in a parallel arrangement to operate the wind tunnel.

B. Description of the Test Section

A sketch of the test section configuration is shown in Figure 1. This test section is the same as was used in the investigation of Reference 1. Figure 3 shows the nozzle contour and the location of static pressure orifices. The undistorted throat cross section was 2.6 inches wide and nominally 0.084 inch high. The distorted throat cross section was 2.6 inches wide with the height varying linearly from 0.084 inch to 0.088 inch. The method of producing the distorted nozzle shape is indicated in Figure 4. Figure 5 shows the measured throat cross sections both before and after distortion.

C. Instrumentation

Instrumentation included a model support system with an axial drive mechanism, a nine-tube Pitot pressure rake, multiple tube mercury and silicone manometers with vacuum reference, a carbon dioxide cooled dew point indicator, a mercury-in-glass thermometer for measuring the stagnation temperature, and a Tate-Emery indicator for measuring the reservoir pressure.

The Pitot pressure rake (Figure 2) was made from 0.032 inch O.D. stainless steel tubing. The rake was mounted in the test section so that the center tube remained on the test section axis throughout the horizontal traversing. The other tubes were spaced 0.25 inch apart in the horizontal plane through the tunnel axis.

D. Test Procedure

Transverse Pitot pressure profiles were obtained from the nine-tube rake at several axial stations between 2 1/2 and 11 1/2 inches downstream from the throat. These profiles were obtained first for the undistorted throat. The lower nozzle block was then removed without disturbing the rake mounting. Material was removed by hand from the throat region of this block as indicated in Figure 4. The block was then mounted in its original position in the test section, and transverse Pitot pressure profiles were obtained for the distorted nozzle at the same axial stations as for the undistorted nozzle described above.

Before each test the actual throat height was measured at several transverse positions by pulling lead wires through the throat. This was done after the side plates had been fastened securely in position, and care was taken not to disturb the nozzle block positioning after this measurement had been made. The results of these measurements are shown in Figure 5.

Static pressures on the centerline of the upper nozzle block were measured at the beginning of each test run with the total head

rake in its most downstream position. Two additional static pressure orifices in the north sideplate at the same axial position (X = 11 inches) and equally spaced above and below the horizontal plane of symmetry were used to indicate symmetry of flow conditions during each run.

All tests were made at a stagnation pressure of 50 psig, stagnation temperatures between 70 and 90°F, and dew points of the reservoir air near -30°F measured at atmospheric pressure.

III. DISCUSSION OF RESULTS

The results of the Pitot pressure measurements are shown in Figures 6 and 7 for the undistorted and distorted throat regions respectively. The general shapes of the profiles are similar in both figures; however, the profiles of Figure 7 appear to be rotated about a point near the centerline as compared to those of Figure 6 for all profiles downstream from X = 2.86 inches. A remarkable feature of the distorted throat Pitot pressure profiles is that they indicate higher Mach numbers downstream from the wider portions of the throat, for all profiles downstream from X = 2.86 inches. One-dimensional isentropic flow relations predict just the opposite condition.

The cause of the waviness of the profiles of Figures 6 and 7 is unknown; however, since the same profile shapes remained after the throat distortion, it is assumed that the cause does not lie in the immediate vicinity of the throat. One possible cause is slight leakage through the static pressure orifices in the upper nozzle block. Inaccessibility of the tubes leading to these orifices prevented positive sealing measures.

In order to show the gross effects of the throat distortion without the effects of the extraneous disturbances, the data points of Figures 6 and 7 were replotted as curves of p'_o / p_o versus X for each of the nine Pitot pressure tubes. Smooth curves were then faired through these points. The constant Mach number contours of Figures 8 and 9 were derived from these faired curves. The fairing removed much of

the effect of the apparently random waviness of the Pitot pressure profiles. The effect due to the throat distortion is obvious in the slopes of the Mach number contours of Figure 9 in contrast to the nearly zero-slope contours of Figure 8.

The magnitude of the effect of the throat distortion is approximately that predicted by one-dimensional isentropic relations. The approximate axial distortion of the Mach number contours as predicted by one-dimensional theory is indicated on Figure 9 for several axial stations. Note that only the magnitude of the distortion is approximately the one-dimensional value, while the slopes of the contours are reversed.

In attempting to understand the apparent reversal of the pressure profiles, linearized supersonic wave theory was applied to the flow in the plane of symmetry with the Mach number distribution assumed to be given by one-dimensional isentropic flow relations (Figure 3). Some of the resultant characteristics (Mach lines) are shown in Figure 10. The scale used in plotting Figure 10 is the same as that used for Figures 8 and 9 in order to facilitate correlation. With such a symmetrical system of Mach lines, one would expect that a pressure profile at any station would be reversed (and possibly distorted) in the distance required for a Mach line to cross the channel. If Figures 9 and 10 are compared, it is seen that this is approximately the case. After the first reversal (in the neighborhood of $X \approx 4$ inches), the Mach lines are quite steep, and are becoming steeper (approaching the flow direction) so that the next reversal of the profile should not occur within the region of this investigation.

PART TWO

AN EXPERIMENTAL INVESTIGATION OF FLOW OVER SIMPLE BLUNT BODIES AT A NOMINAL MACH NUMBER OF 5.8

I. INTRODUCTION

In the development of long-range, high speed missiles the problem of aerodynamic heating has become of primary importance. Missiles traveling at moderate supersonic speeds (Mach number greater than 3) can encounter local recovery temperatures above $600^{\circ}F$ so that unless adequate provision is made for the removal of heat from the critical areas, the structure of the missile is considerably weakened. As the speed of the missile is increased into the high supersonic and hypersonic range, local recovery temperatures are encountered which would not only weaken structural elements but would melt or vaporize common materials used in missile construction.

The apparatus which removes heat from critical regions on a missile will occupy space, whether the apparatus consists of a large mass for heat absorption, liquid coolant, or gas coolant. As the speed and range of the missile increase, the heat removal apparatus must be increased accordingly. This necessity for a large structural volume in the regions of high recovery temperatures dictates blunt noses for very high-speed, long-range missiles, even though this might result in a sacrifice in aerodynamic performance due to the increased drag. This increase in drag can be an advantage in itself since it will tend to decelerate a missile prior to its re-entry into the denser portion of the atmosphere, thus reducing the heat transfer to the missile surface.

Theoretical analysis of hypersonic flow about blunt bodies is complicated in many practical cases by the presence of mixed flow conditions. In cases where a detached shock wave is produced, the

flow behind the shock wave consists of subsonic, sonic, and supersonic flow. Some configurations produce flows which separate from the body surface, making a complete theoretical treatment impossible.

In hypersonic flow, shock waves lie close to the body surface so that changes in flow properties from free stream values occur in a thin region near the body surface. The Newtonian Theory (see Appendix) treats the fluid as being composed of discrete particles with no interaction between particles. This idealized fluid is unperturbed prior to its contact with a body surface. Upon striking the body surface, each particle loses the component of its momentum which is normal to the body surface. This momentum is transferred to the body surface, producing a surface static pressure, p_s, higher than the free stream static pressure, p_∞, by an amount, $p_s - p_\infty = \rho_\infty U_\infty^2 \cos^2 \eta$, where ρ_∞ is the mass density of the fluid in the free stream, η is the angle between the free stream flow direction and the normal to the body surface, and U_∞ is the free stream velocity.

This investigation was undertaken to provide experimental data for flows about some simple blunt body configurations at a nominal Mach number of 5.8. The bodies selected for this investigation were simple geometric shapes which were expected to produce flows involving attached shocks, detached shocks, and separation. Where no separation exists, the experimental results should provide a test of the simple Newtonian concept.

II. EQUIPMENT AND PROCEDURE

A. Wind Tunnel Description

The present investigation was conducted in the GALCIT 5" x 5" Hypersonic Wind Tunnel (Leg No. 1). This is a continuously-operating, closed return tunnel consisting of thirteen rotary vane-type positive-displacement compressors; three reciprocating piston type compressors; a silica-gel dryer for water removal; Cyclone separators, activated carbon cannisters, and fiberglass filters for oil removal; a steam heat exchanger for obtaining the required reservoir stagnation temperature; coolers to reduce the air temperatures before entry into the compressors; and the necessary piping and valving to permit a variety of operating arrangements. For this investigation the plant was operated with five stages of compression, utilizing the thirteen vane-type compressors only.

The test section of Leg No. 1 consists of two solid steel nozzle blocks, an integral lower diffuser block and center block, an upper center block, an upper diffuser block, and two steel side-plates with six removable ports in each for schlieren observation or instrumentation leads. (See Figure 11)

B. Model Description

1. 40° Half-Angle Cone (See Figure 12)

Two 40° half-angle cone models were used for determining surface static pressure distributions. The models differ only in static pressure

orifice distribution. On one model the pressure orifices are placed on one ray while on the other model the orifices are staggered so that two orifices appear on each of four rays at 90° intervals about the cone. Both models are made of brass with a nominal base diameter of one inch.

The orifices and pressure leads were made integral by silver soldering 0.032 inch O.D. X 0.006 inch wall stainless steel tubing into the models prior to the final machining. One end of the stainless tubing is flush with the model surface, forming a 0.020 inch diameter orifice. This tube then extends approximately two inches downstream from the rear of the model support shaft where a connection is made with Saran tubing. This construction eliminates soldered joints within the body of the model and thus reduces the possibility of leaks in inaccessible places.

2. 40° Half-Angle Cone with Spherical Nose (See Figure 13)

The spherical-nosed 40° half-angle cone model is made of brass with a nominal base diameter of one inch. Its construction is similar to that of the cone model described above. The nose radius is 0.20 inch, resulting in a ratio of nose radius to base radius of 0.4. A thermocouple was buried in the model, as indicated in Figure 13. This thermocouple indicates the temperature of the surface. Its leads extend into the body of the model and out through the support shaft with the pressure leads.

3. Hemisphere-Cylinder (See Figure 14)

The hemisphere-cylinder model is made of brass and has a nominal diameter of one inch. The length of the cylindrical afterbody is

approximately one-half the diameter. Eight static pressure orifices are placed at approximately 15° intervals along one ray of the hemisphere, one orifice being on the major axis of the model. Four additional orifices are spaced at about 0.1 inch intervals along the extension of this same ray on the cylindrical afterbody. The pressure lead details are similar to those of the 40° half-angle cone described above.

4. 10° - 40° Half-Angle Double Cone (See Figure 15)

The 10° - 40° half-angle double cone model is made of brass and consists of a 10° half-angle conical nose 5/8 inch long (measured along the axis) and a one inch base diameter, 40° half-angle, conical afterbody. The nose cone was made separately from the afterbody. Five holes were drilled into the base of the nose cone, and 0.032 inch O.D. stainless steel tubes were silver soldered into these holes. 0.013 inch diameter holes were then drilled normal to the cone surface to meet the holes drilled in the base. The afterbody was constructed in a manner similar to that described above for the 40° half-angle cone, and the nose cone was silver soldered in place. The model was then machined to its final dimensions.

5. 13°-30° Half-Angle Double Cone (See Figure 16)

The 13° - 30° half-angle double cone model is made of stainless steel and consists of a 13° half-angle nose cone 1.67 inches long, a 0.87 inch long conical center section with a 30° half-angle, and a 10° half-angle rear section 2.35 inches long. The maximum body diameter (at the rear of the center section) is 1.77 inches. This model contains no pressure leads since it was used for schlieren observation only.

6. Flat-Nosed Circular Cylinder (See Figure 17)

The flat-nosed cylinder model is made of brass and has a nominal diameter of one inch. Seven static pressure orifices are placed along one radius on the flat nose. Four more orifices are located on the after-body in pairs. The two orifices of each pair are placed at the same distance from the model nose and are diametrically opposite on the cylinder. These orifices were used to give an indication of alignment of the model with respect to the free stream flow direction in the tunnel.

7. Circular Cylinder with Its Major Axis Normal to the Free Stream Flow Direction (See Figure 18)

Two brass models were built for investigating the flow about a circular cylinder with its major axis normal to the free stream flow direction. One model was used for schlieren observation, and the other was used for surface static pressure measurements. Both models have a diameter of 0.715 inch and are 5 inches long. The models were placed horizontally across the test section of Leg No. 1 at the center of the third pair of window ports (see Figure 11).

The static pressure model (Figure 18A) was mounted between two solid steel ports with the static pressure leads extending out through one end of the model and through the side port. "O-ring" seals were used on the model extensions to prevent leakage into the holes through the ports. A pointer connected to the model and on the outside of the port was used for positioning the number two orifice on the stagnation streamline while the tunnel was operating.

For schlieren observation a dummy model was made with the same diameter as that of the pressure model (see Figure 18B). This model was mounted on two thin brass strips adjacent to the tunnel side plates. These strips extended downstream to the center of the next pair of ports (solid) where they were soldered to lugs which in turn were attached to the ports. (See Figure 11)

C. Procedure

1. Model Mounting and Leak Checking

The models were mounted in the test section from 22 to 24 inches downstream from the nozzle throat in a region of uniform flow conditions as determined by previous static pressure calibration surveys. All models, except the circular cylinder normal to the free stream flow, were mounted on a 1/2" square steel bar on the vertical model-actuator struts at zero angles of attack and yaw. The vertical actuators can be moved independently so that minor corrections to angle of attack could be made during tunnel operation. The model support stings between the 1/2" square bar and the models were designed according to Reference 2 to insure a negligible effect of the sting dimensions on the static pressure readings.

The model pressure leads were connected to Saran tubing inside the test section of the tunnel. The Saran leads passed through "O-ring" seals in a side port and were in turn attached to copper tubing leading to the manometers. Leak checking was performed by evacuating the pressure lead and manometer tube, then clamping off the vacuum pump.

A pressure rise in the system, indicating leakage, was indicated by a movement of the manometer fluid.

2. Tunnel Operation and Control

After the compressor plant was started, approximately 1 1/2 hours of tunnel operation at a stagnation pressure of 80 psig. were required for equilibrium temperature conditions to be established in the test section. This time was determined by observing the temperature on the surface of the spherical-nosed cone model (Figure 13). No static pressure measurements were made until the tunnel had been operating at least 1 1/2 hours.

The tunnel reservoir pressure was controlled by a Minneapolis-Honeywell-Brown circular chart controller within $\pm$ 0.04 psi and was measured with a Tate-Emery nitrogen-balanced gage.

The tunnel stagnation temperature was indicated, recorded, and controlled by a Minneapolis-Honeywell-Brown circular chart controller within $\pm 2^{\circ}F$. The temperature sensing element is an iron-constantan schielded thermocouple placed one inch upstream from the nozzle throat.

III. DISCUSSION OF RESULTS

A. Schlieren Observation

1. General

The schlieren photographs show shock waves very near the body surfaces, as would be predicted by inviscid hypersonic theory. This condition is less pronounced in the two-dimensional case of the circular cylinder normal to the free stream flow direction. From this we would expect closer correlation between Newtonian theory and experimental observation for bodies of revolution than for two-dimensional bodies. The pressure measurements of this investigation indicate that this is true.

2. 40° Half-Angle Cone

Figure 19 is a schlieren photograph of the 40° half-angle cone model at a free stream Mach number of 5.8 and a free stream Reynolds number per inch of 2.38×10^{5}. The shock wave is attached, and the shock wave angle measures 47°. Inviscid flow theory (Kopal, Reference 4) gives a shock wave angle of 46.6° for this case.

3. Spherical-Nosed 40° Half-Angle Cone

Figure 20 is a schlieren photograph of the spherical-nosed 40° half-angle cone at the same free stream conditions as those for the cone described above. The detached bow wave is very close to the body surface, and the shock wave angle rapidly approaches the wave angle for a 40° half-angle cone.

4. Hemisphere-Cylinder

The schlieren photograph of the hemisphere-cylinder model (Figure 21) shows a detached shock wave which is relatively close to the body surface.

5. Circular Cylinder Transverse to the Free Stream (Figure 22)

The shock wave of the circular cylinder transverse to the free-stream flow direction is relatively much farther from the body surface than in the case of the hemisphere. Oil on the windows is noticeable in the photograph and gives a false indication of separation upstream from the cylinder axis. However, the static pressure data shows the separation point to be slightly downstream from the cylinder axis.

6. 13° - 30° Half-Angle Double Cone

Figures 23 and 24 show the 13° - 30° half-angle double cone at free stream Reynolds numbers per inch of 2.4×10^5 and 0.65×10^5, respectively. Separation (dark area adjacent to the body in the lower half of the photograph) occurs somewhat earlier in Figure 23 probably because of the higher Reynolds number. A discontinuity surface is evident in the lower right hand corner of Figure 23 between the body surface and the shock wave. The air between this surface and the body has passed through three relatively-weak oblique shocks, while the air between this surface and the shock wave has passed through one strong shock. This surface then shows the direction of the streamlines in its vicinity.

7. 10° - 40° Half-Angle Double Cone

The schlieren photograph of the 10° - 40° half-angle double cone (Figure 25) shows that separation occurs very near the nose, producing an effective half cone angle of 21°. (See Figure 29). In this photograph, as in Figure 23, a discontinuity surface is evident between the body surface and the strong shock wave near the trailing edge of the model.

8. Flat-Nosed Circular Cylinder

The shock wave of the flat-nosed circular cylinder with its major axis parallel to the free stream flow direction is shown in Figure 26. The shock wave is nearly normal over the entire face of the body. The shape of the upstream portion of the shock wave closely approximates a sphere with a radius of two inches.

B. Static Pressure Measurements

1. General

According to Newton's concept, the pressure coefficient on the surface of a body is given by $C_p = 2 \cos^2 \eta$, where η is the angle between the normal to the surface element and the free stream flow direction. For an unyawed hemisphere $\eta = \theta$, where θ is the ray angle measured from the stagnation point. In the "modern" theory of inviscid hypersonic flow, Newton's expression is strictly correct in the limiting case $M_\infty \sin \theta \to \infty$ and $\gamma \to 1$. For a real gas at a finite but high Mach number the pressure coefficient $C_{p_{max}}$ at the stagnation point (for example) is given by

$$C_{p_{max}} = 2 - \frac{\rho_\infty}{\rho_2} = \frac{\gamma + 3}{\gamma + 1}\left[1 - \frac{2}{\gamma + 3}\,\frac{1}{M_\infty^2}\right]$$

which is less than the value 2.0 predicted by Newton. The closeness of the bow shock wave and the body surface suggests that the $\cos^2 \eta$ "law" is a good approximation but that it would be more revealing to compare the ratio $C_p / C_{p_{max}}$ with $\cos^2 \eta$.

In general, the results of the static pressure investigation indicate good agreement with the modified Newtonian expression (above) for the bodies of revolution and fair agreement for the two-dimensional body (circular cylinder transverse to the flow).

2. 40° Half-Angle Cone

The pressure coefficient distributions for the 40° half-angle cone are given in Figure 27 for free stream Reynolds numbers of 0.65×10^5, 1.22×10^5, and 1.38×10^5. The measured values of the pressure coefficient are fairly well confined between the inviscid theory (Kopal) values and the Newtonian theory values.

3. Spherical-Nosed 40° Half-Angle Cone

Figure 28 shows the experimental pressure coefficient distributions at three Reynolds numbers. The modified Newtonian expression $C_p / C_{p_{max}} = \cos^2 \theta$ gives a fair approximation to the distribution, as does inviscid theory (Kopal, Reference 4) for the conical portion of the model. There is a slight overexpansion of the air downstream from the beginning of the conical section, but the pressure then rises

rapidly and approaches the inviscid theory value. Here, as in the case of the 40° half-angle cone, the Newtonian theory gives a slightly lower value of the pressure coefficient than is found experimentally.

4. 10° - 40° Half-Angle Double Cone

Figure 29 presents the results of surface pressure measurements on the 10° - 40° half-angle double cone at Reynolds numbers from 0.65×10^5 to 2.38×10^5. The sketch at the top of Figure 29 was made from the schlieren photograph (Figure 25) and shows that separation starts very near the nose, forming an effective half cone angle of 21°. The inviscid theory (Kopal) value of the pressure coefficient for a 21° half-angle cone is included in Figure 29 and shows excellent agreement with the measured value over most of the separated region. The experimentally-determined pressure coefficients for the low Reynolds number case ($P_o = 10.0$ psig) indicate separation downstream from the first orifice.

5. Hemisphere-Cylinder

Figure 30 shows the excellent agreement between the modified Newtonian theory and the experimental results. In this case the agreement appears to be independent of Reynolds number over the range covered in this investigation.

6. Circular Cylinder Transverse to the Free Stream Flow

The correlation between Newtonian theory and experimental results is not so close in the two-dimensional case of the circular

cylinder transverse to the free stream flow (Figure 31) as it is for the hemisphere. The effect of Reynolds number is also somewhat more apparent in this case.

7. Flat-Nosed Circular Cylinder with Its Major Axis Parallel to the Free Stream Flow Direction

Figure 32 shows the pressure coefficient distribution on the flat face of a circular cylinder with its major axis parallel to the free stream flow direction and shows a very flat profile, as would be expected from Newtonian theory. A curious dip was observed in the pressure profile at the center of the face of the model. The absolute magnitude of the pressure decrease at the cylinder axis is just slightly larger than the combined reading and instrument error for two orifices, so a more extensive investigation might clear up this apparent anomaly.

REFERENCES

1. Oliver, R. E., and Nagamatsu, H. T.: Investigation of Flow in the Throat Region for a Hypersonic Nozzle. GALCIT Hypersonic Wind Tunnel Memorandum No. 24, January 15, 1955.

2. Harkins, W. D.: Base Pressure and Static Pressure for a Cone-Cylinder at a Nominal Mach Number of 5.8. GALCIT Hypersonic Wind Tunnel Memorandum No. 19, July, 1954.

3. Shapiro, A. H.: The Dynamics and Thermodynamics of Compressible Fluid Flow. Vol. I, The Ronald Press Co., New York, 1953.

4. Equations, Tables, and Charts for Compressible Flow. National Advisory Committee for Aeronautics, Report No. 1135, 1953.

APPENDIX

The basis for the Newtonian theory (Reference 3) is the assumption that the fluid is undisturbed until it strikes the surface of a body in the flow. Upon striking the body surface the fluid loses the component of its momentum which is normal to the body surface while the tangential component is unchanged. Referring to the sketch below, it can be seen that the component of momentum (per unit volume) normal to the body surface element dA is $\rho_\infty U_\infty \cos\eta$ where η is the angle between the free stream velocity and the normal to the body surface element. The volume of fluid striking the surface per unit time is $U_\infty dA \cos\eta$ so that the net transfer of momentum to the body surface per unit time, per unit surface area, is $\rho_\infty U_\infty^2 \cos^2\eta$. This time rate of momentum transfer per unit area is equal to the difference between the surface static pressure and the free stream static pressure $(p_s - p_\infty)$. The pressure coefficient C_p is defined as $(p_s - p_\infty)\Big/\frac{1}{2}\rho_\infty U_\infty^2$, so the Newtonian theory gives:

$$C_p = 2\cos^2\eta$$

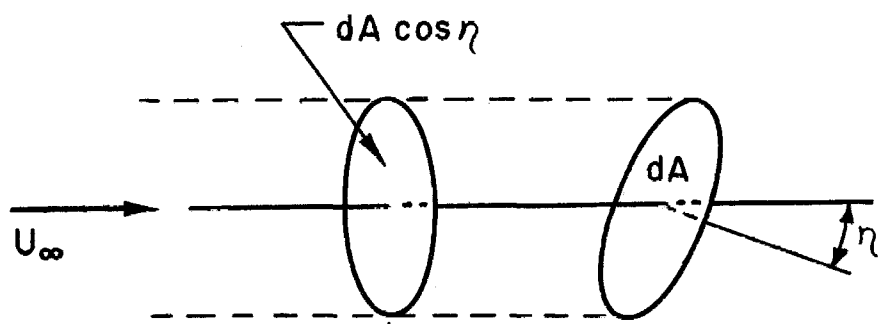

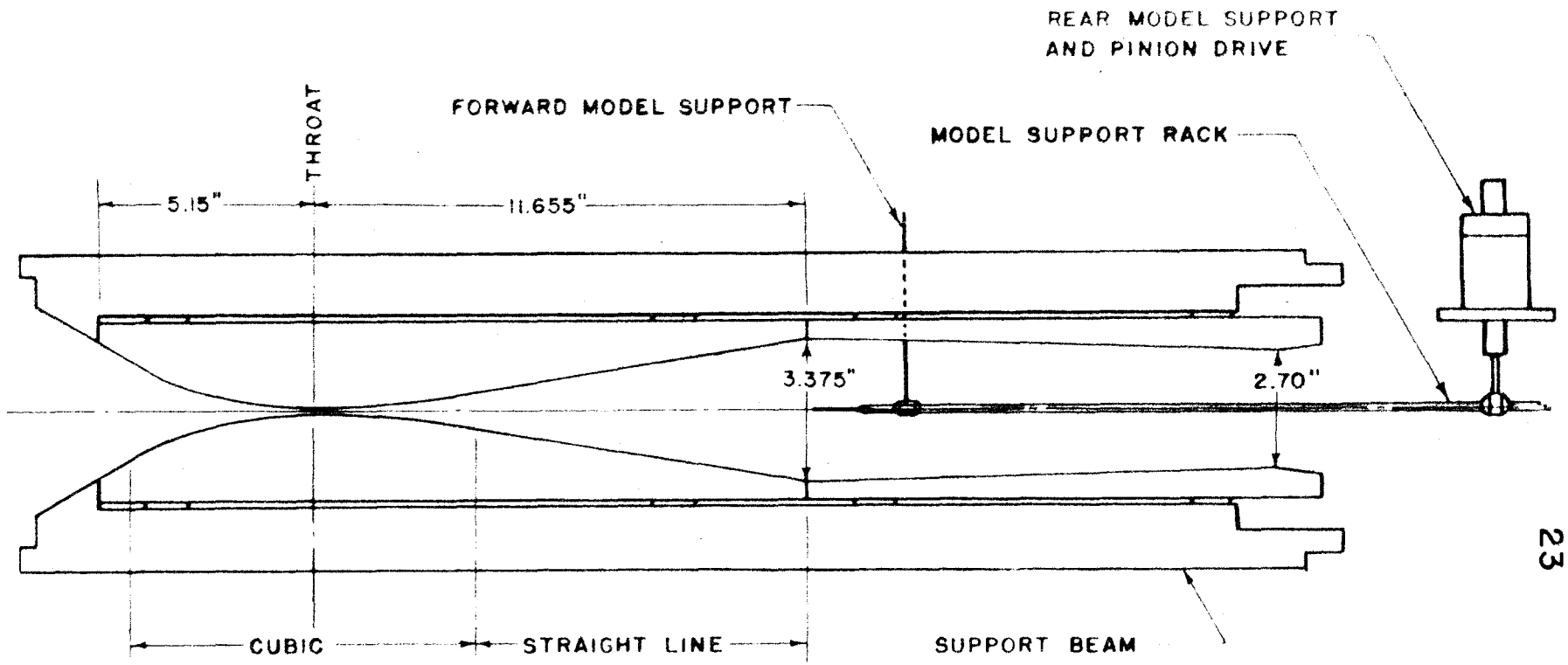

THROAT HEIGHT: 0.084"
NOZZLE WIDTH: 2.57"
THROAT RADIUS: 12"

FIG. 1

TEST SECTION CONFIGURATION

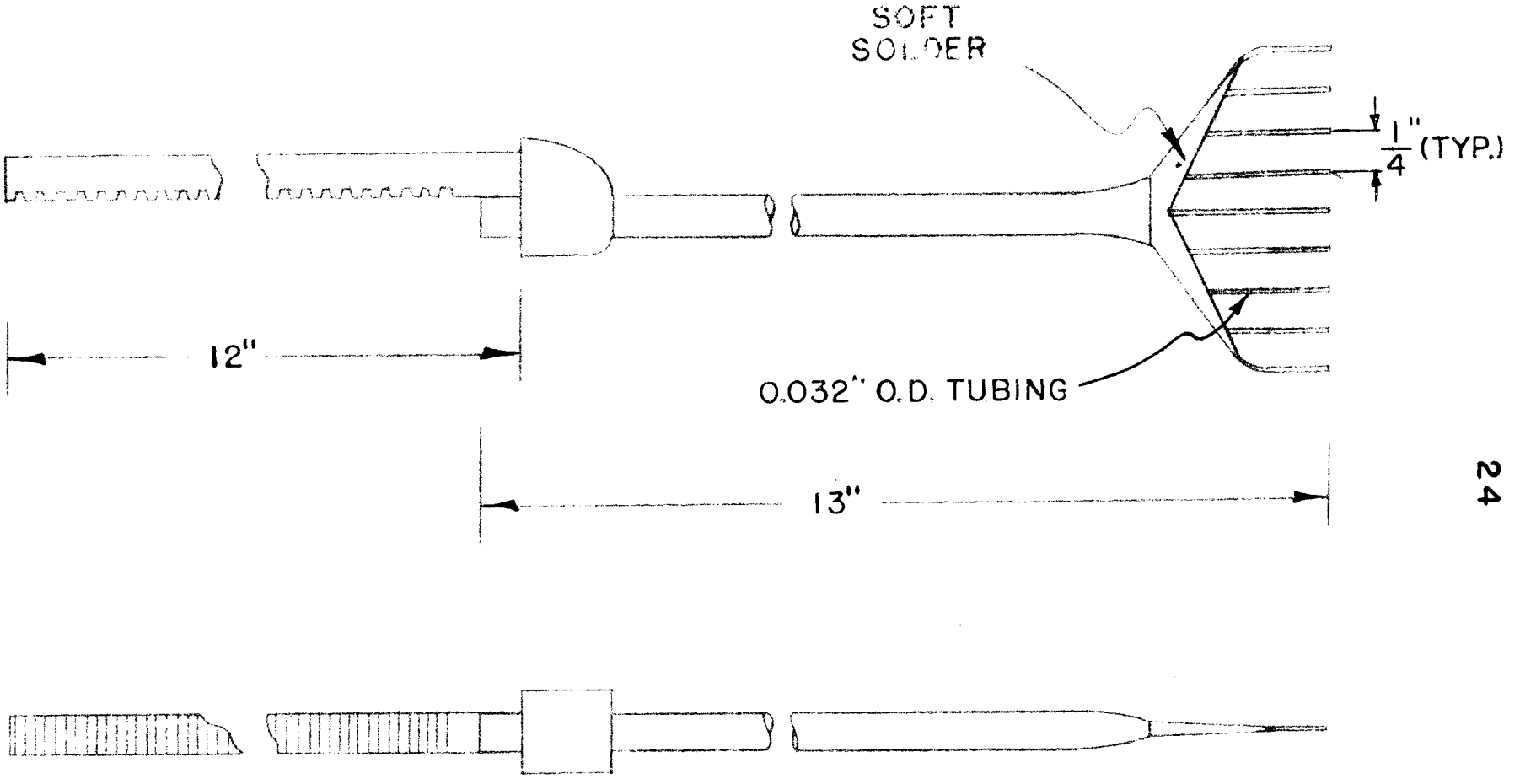

PITOT PRESSURE RAKE

FIG. 2

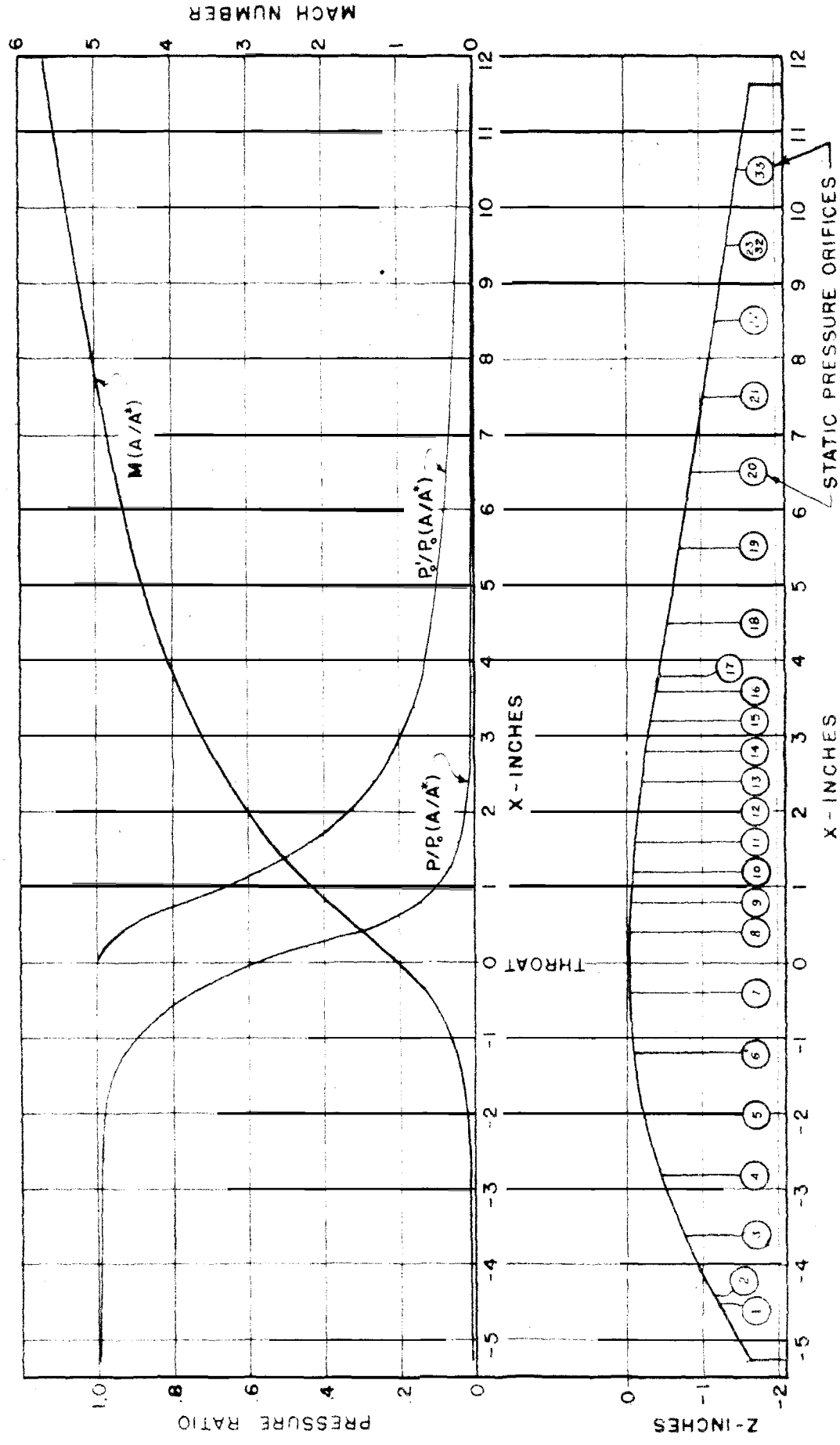

FIG. 3
ISENTROPIC NOZZLE RELATIONS

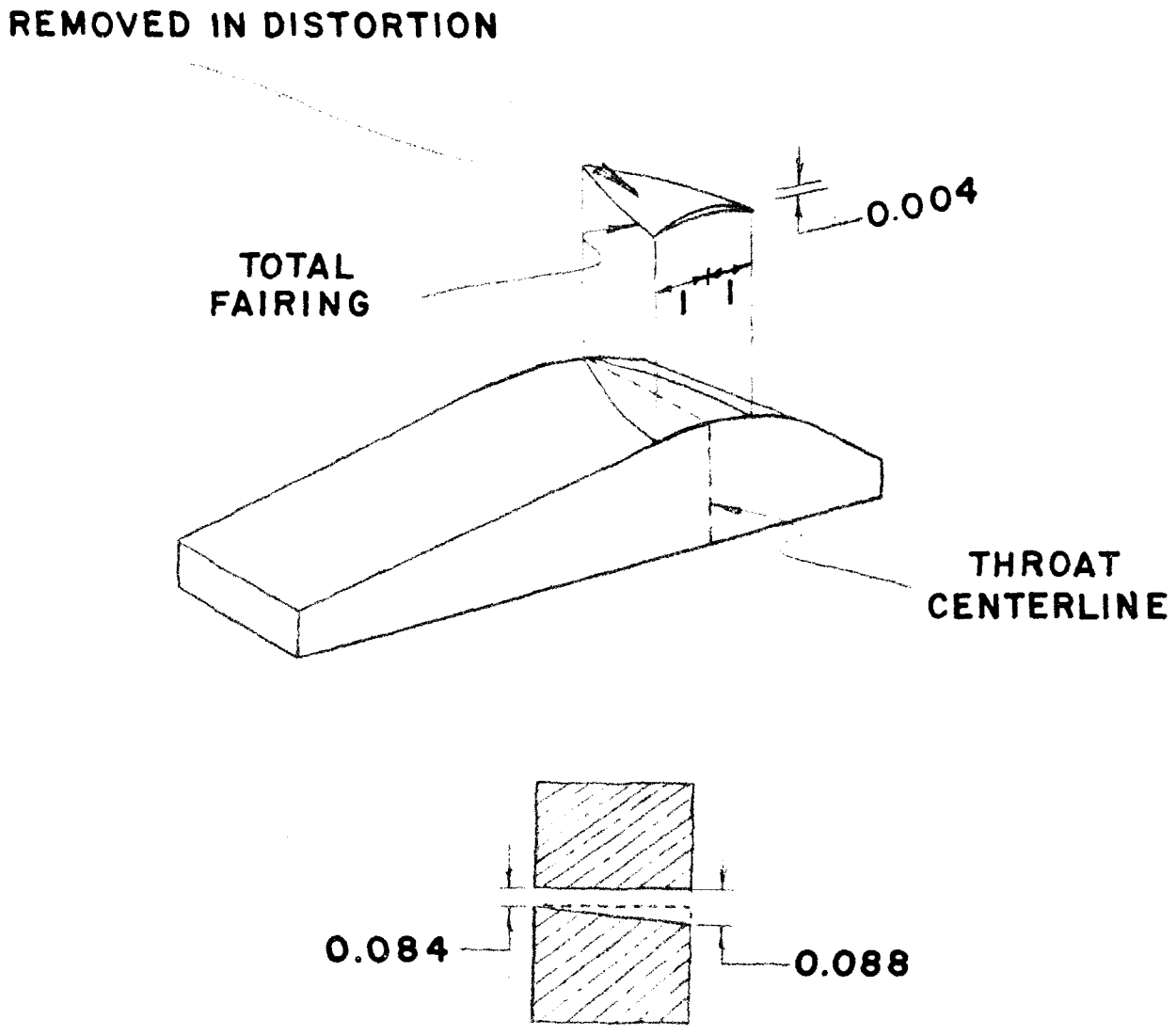

NOZZLE DISTORTION

FIG. 4

THROAT HEIGHT MEASUREMENTS

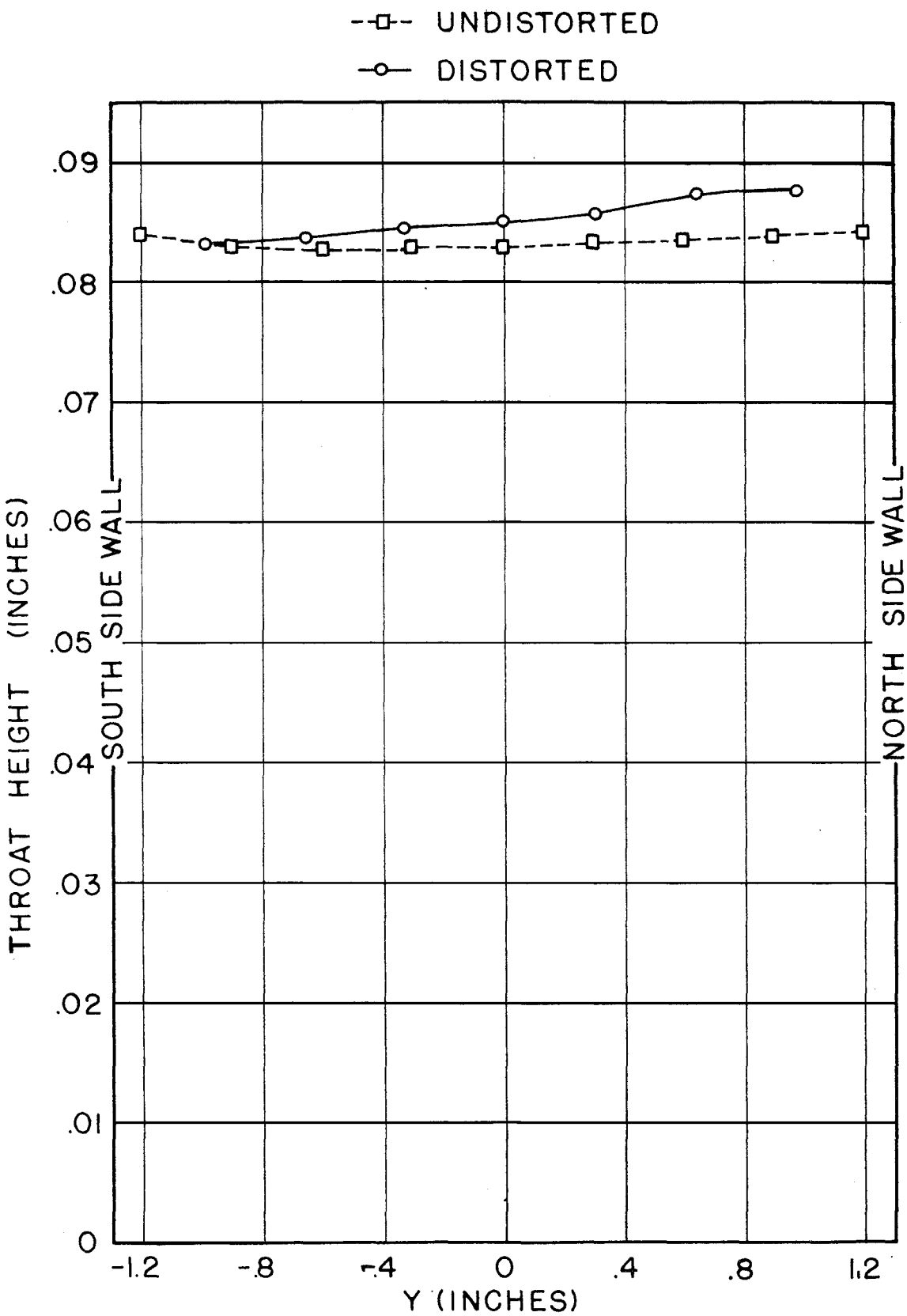

FIG. 5

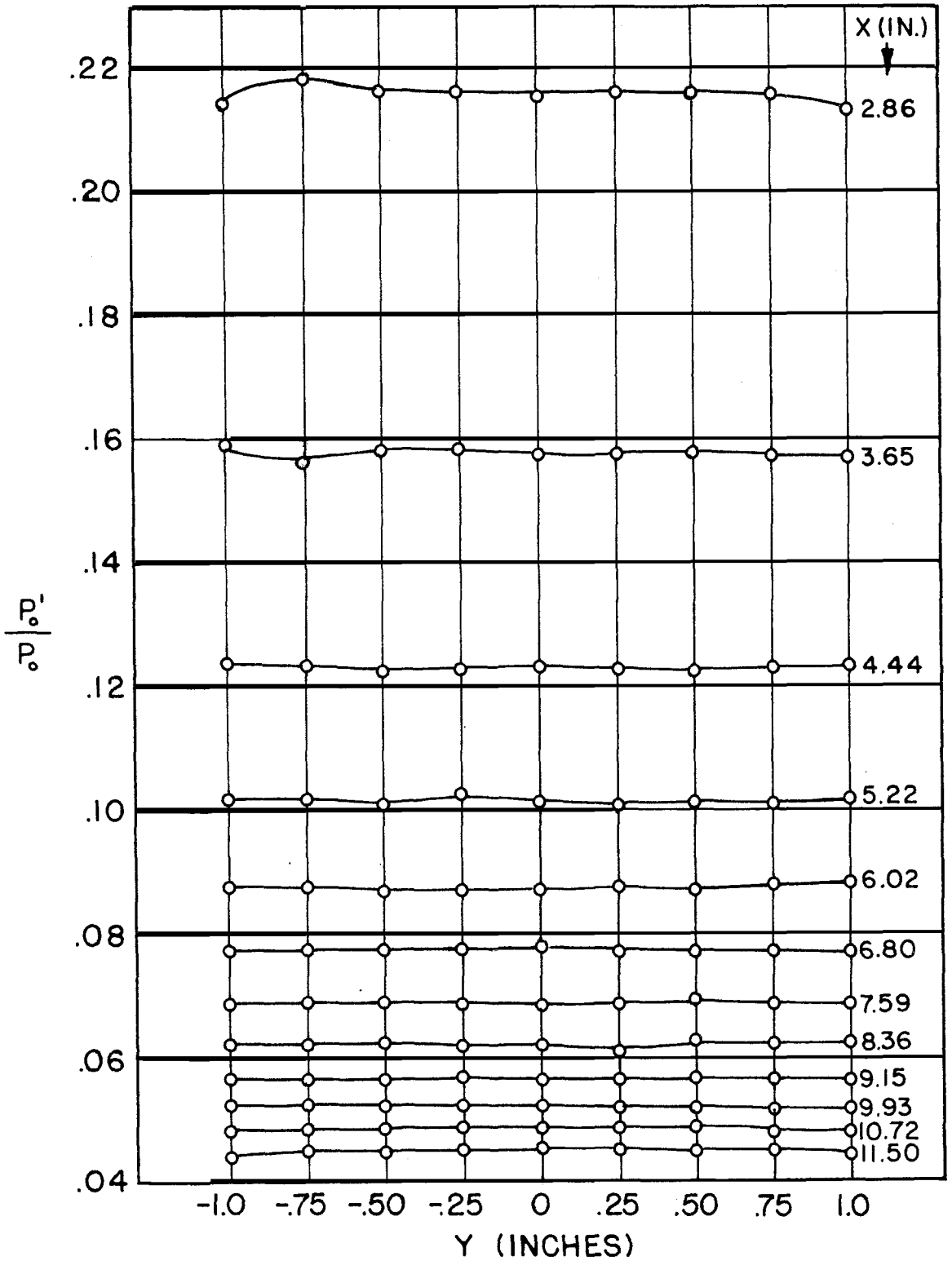

PITOT PRESSURE PROFILES (UNDISTORTED THROAT)

FIG. 6

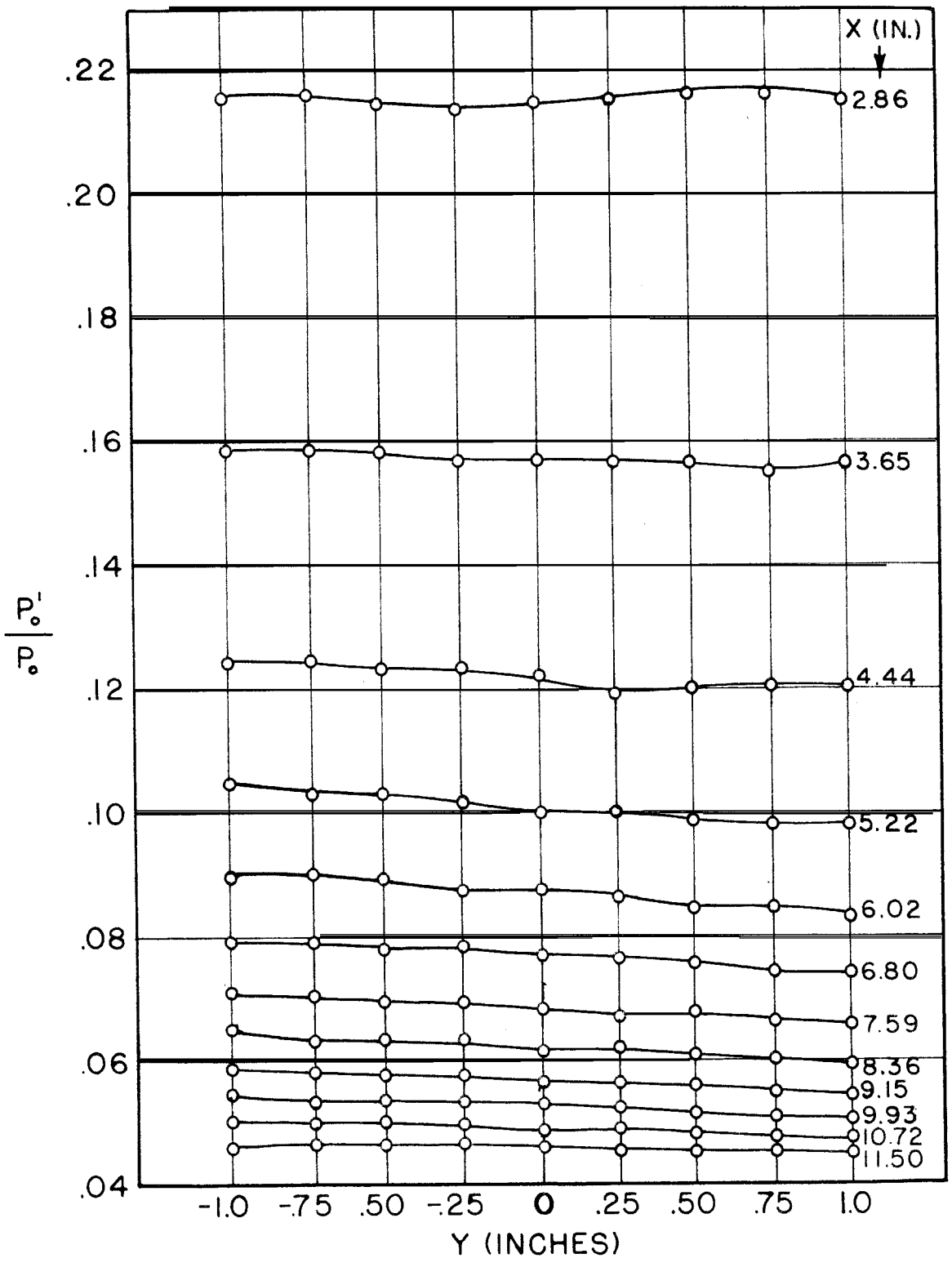

PITOT PRESSURE PROFILES (DISTORTED THROAT)

FIG. 7

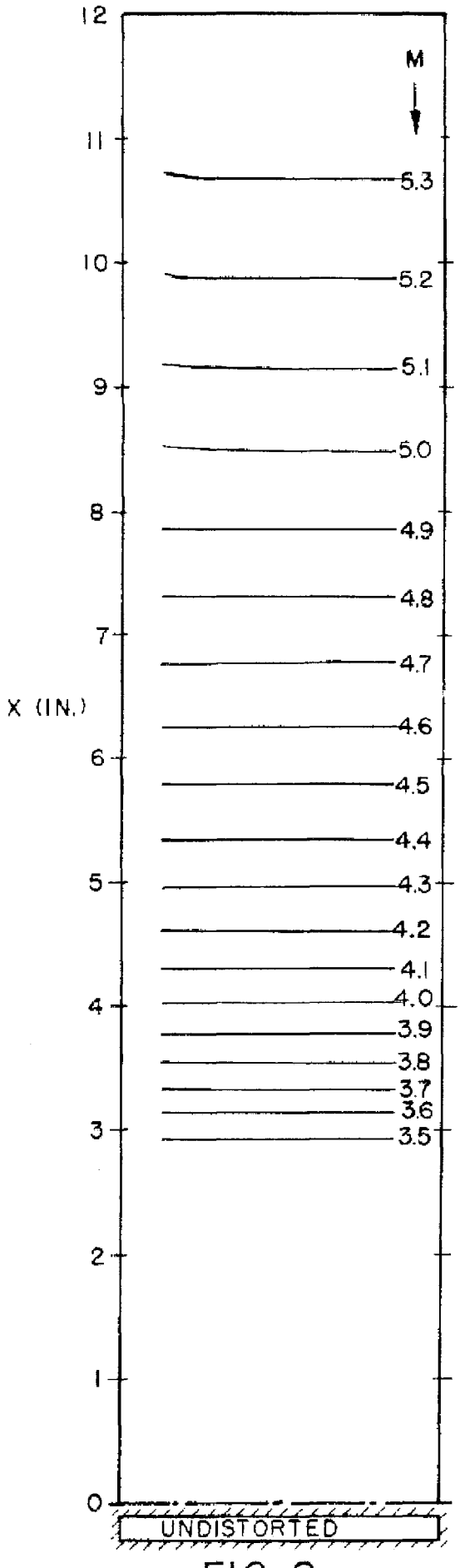

FIG. 8

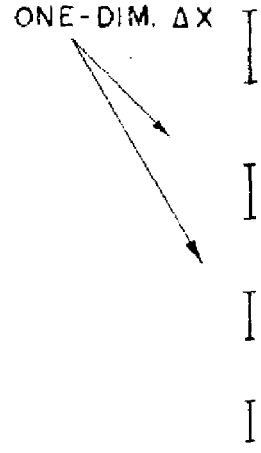

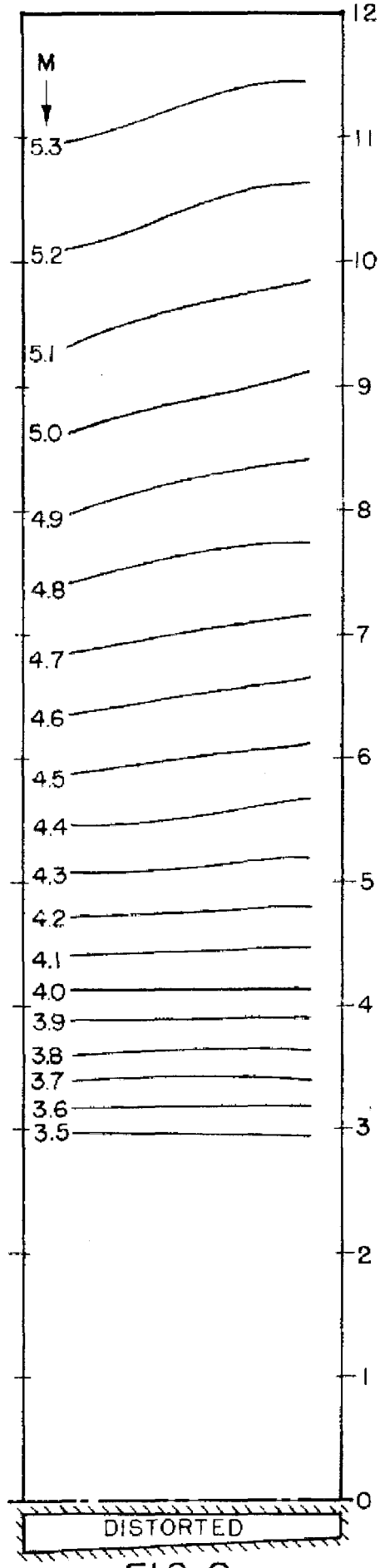

FIG. 9

CONSTANT MACH NUMBER CONTOURS

APPROXIMATE CHARACTERISTICS

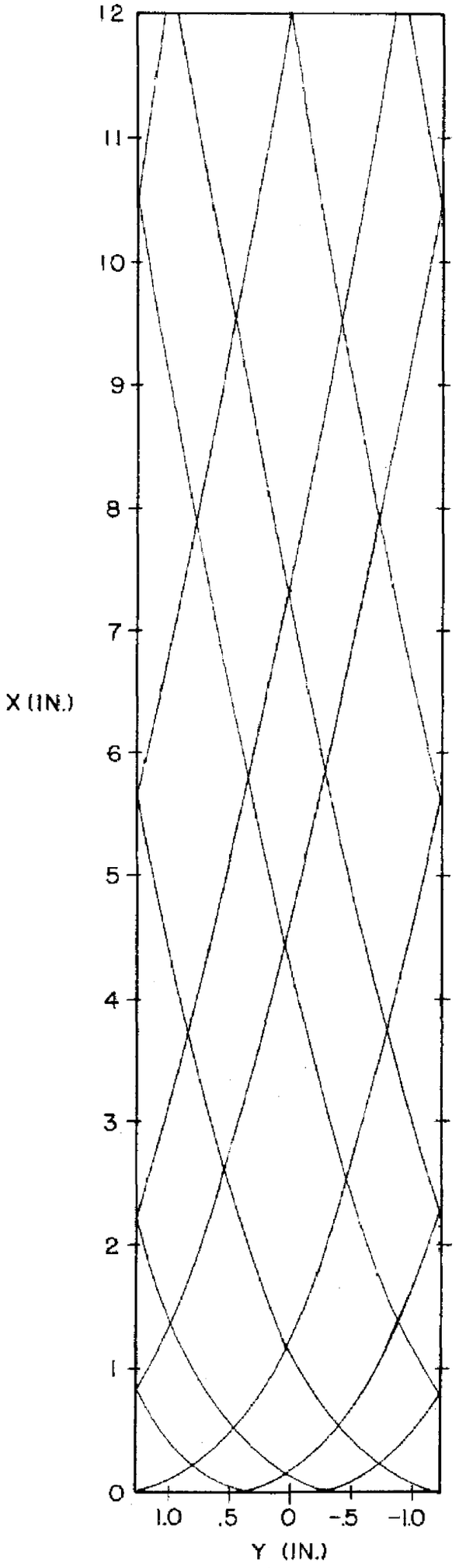

FIG. 10

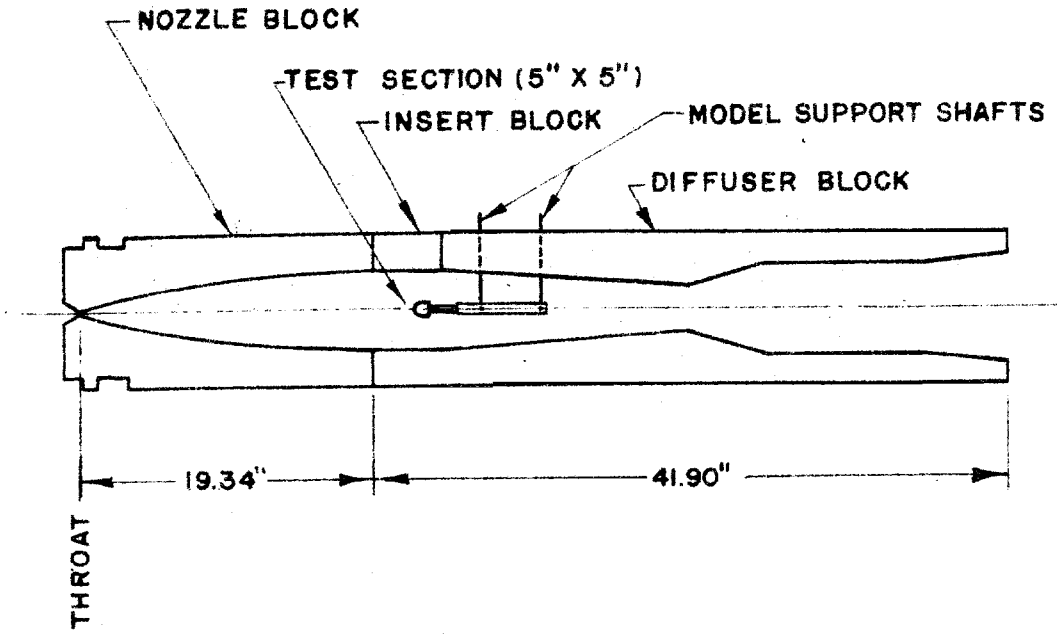

(A) SIDE PLATES REMOVED

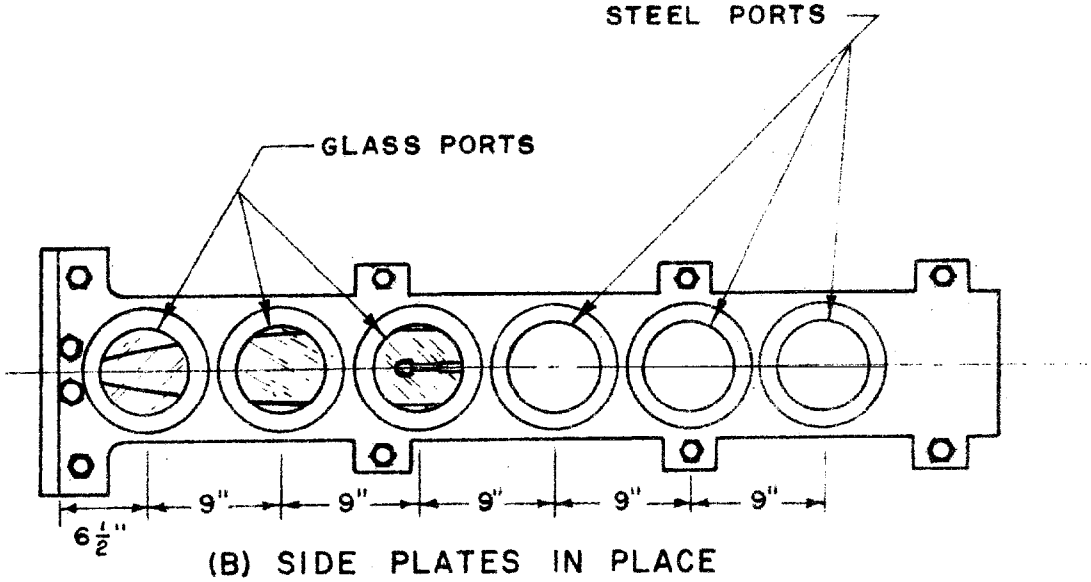

(B) SIDE PLATES IN PLACE

TEST SECTION OF LEG ONE
GALCIT HYPERSONIC WIND TUNNEL

FIGURE 11

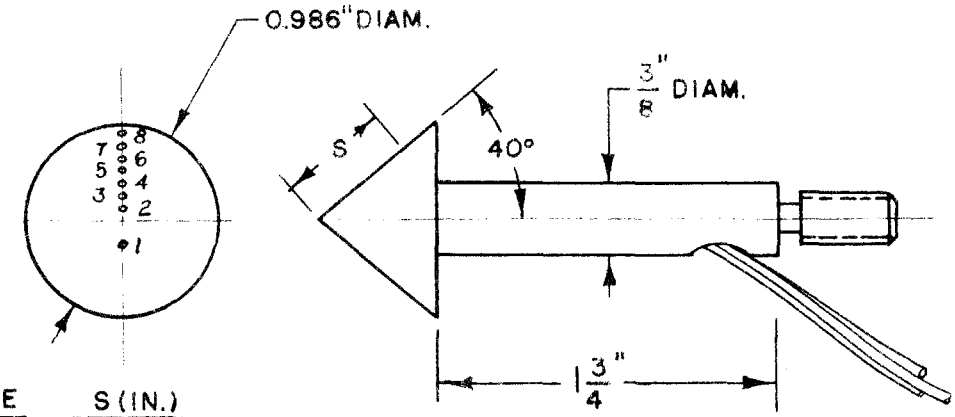

ORIFICE	S (IN.)
1	0.235
2	0.120
3	0.220
4	0.310
5	0.415
6	0.525
7	0.615
8	0.700

(A) 40° HALF-ANGLE CONE
ORIFICES ON ONE RAY

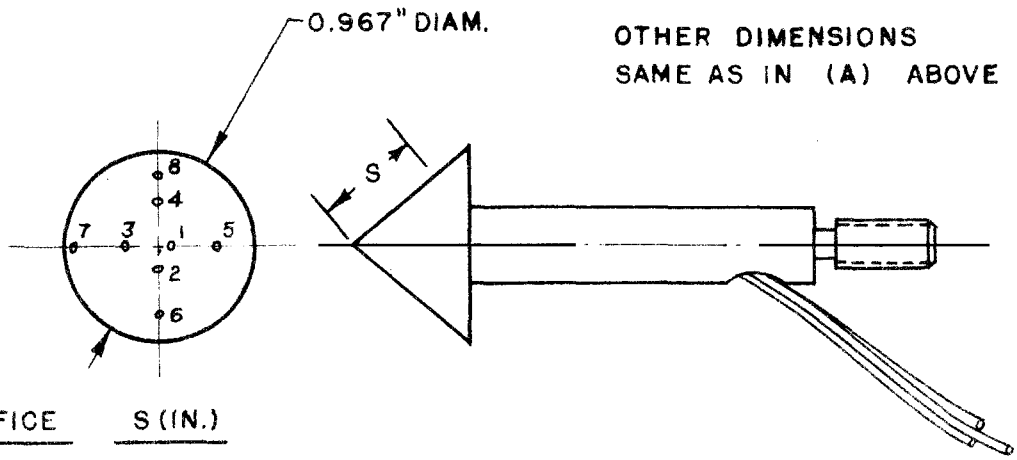

ORIFICE	S (IN.)
1	0.100
2	0.160
3	0.265
4	0.375
5	0.460
6	0.550
7	0.675
8	0.575

(B) 40° HALF-ANGLE CONE
STAGGERED ORIFICES

FIGURE 12

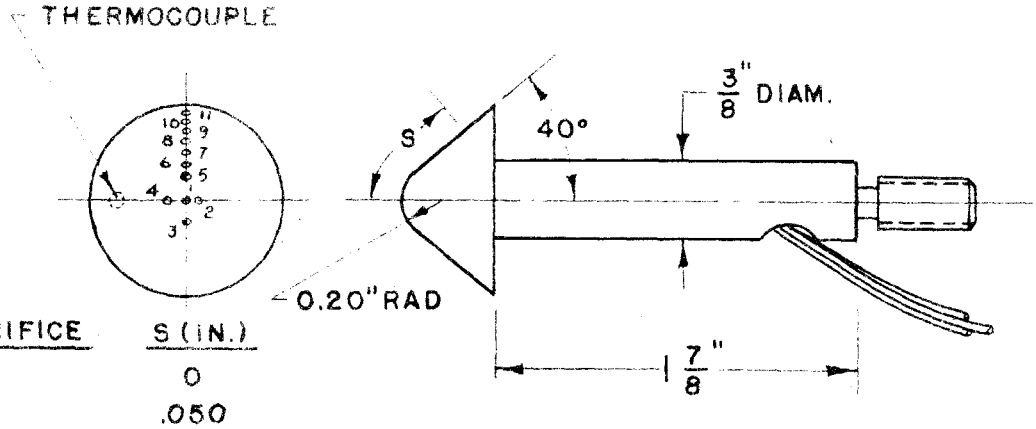

ORIFICE	S (IN.)
1	0
2	.050
3	.067
4	.089
5	.100
6	.164
7	.264
8	.364
9	.464
10	.564
11	.652
THERMOCOUPLE	.395

40° HALF-ANGLE CONE WITH SPHERICAL NOSE

FIGURE 13

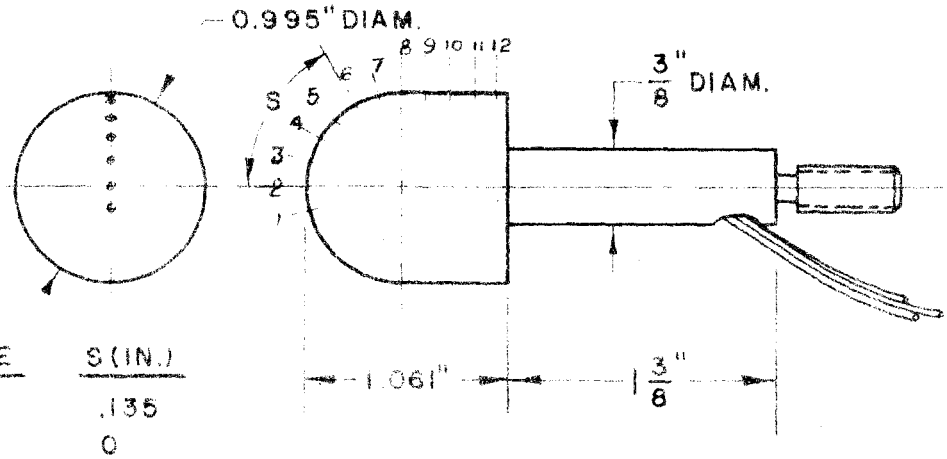

ORIFICE	S (IN.)
1	.135
2	0
3	.108
4	.252
5	.379
6	.509
7	.646
8	.780
9	.899
10	1.032
11	1.153
12	1.269

HEMISPHERE - CYLINDER

FIGURE 14

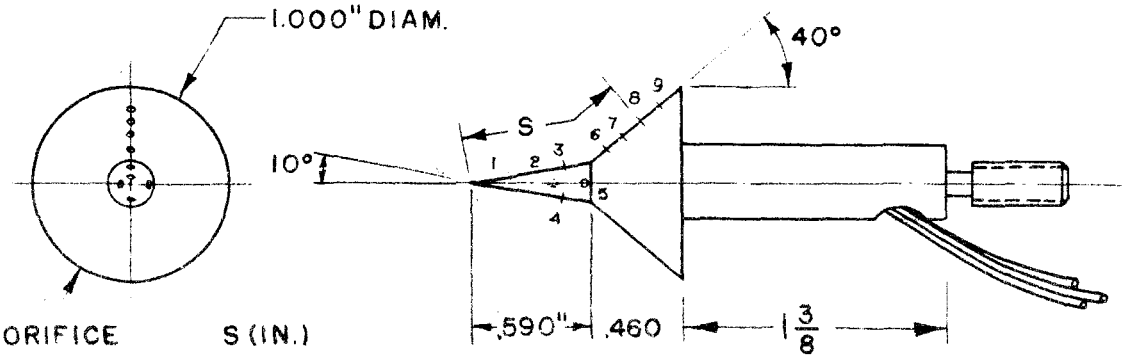

ORIFICE	S (IN.)
1	.200
2	.400
3	.512
4	.514
5	.610
6	.712
7	.818
8	.929
9	1.026

10°-40° HALF-ANGLE DOUBLE CONE

FIGURE 15

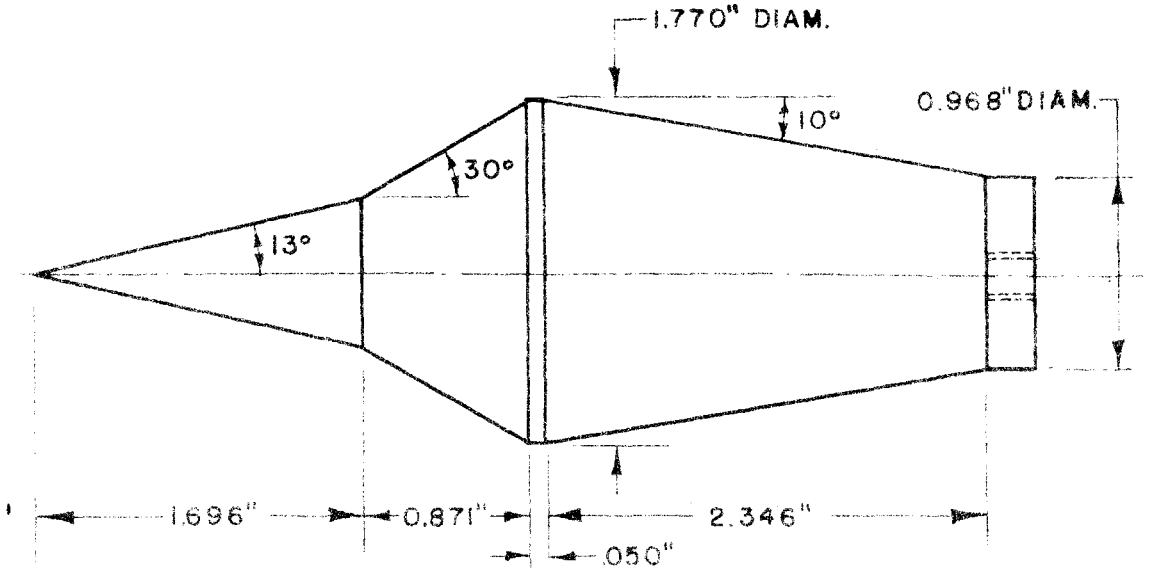

13°-30° HALF-ANGLE DOUBLE CONE

FIGURE 16

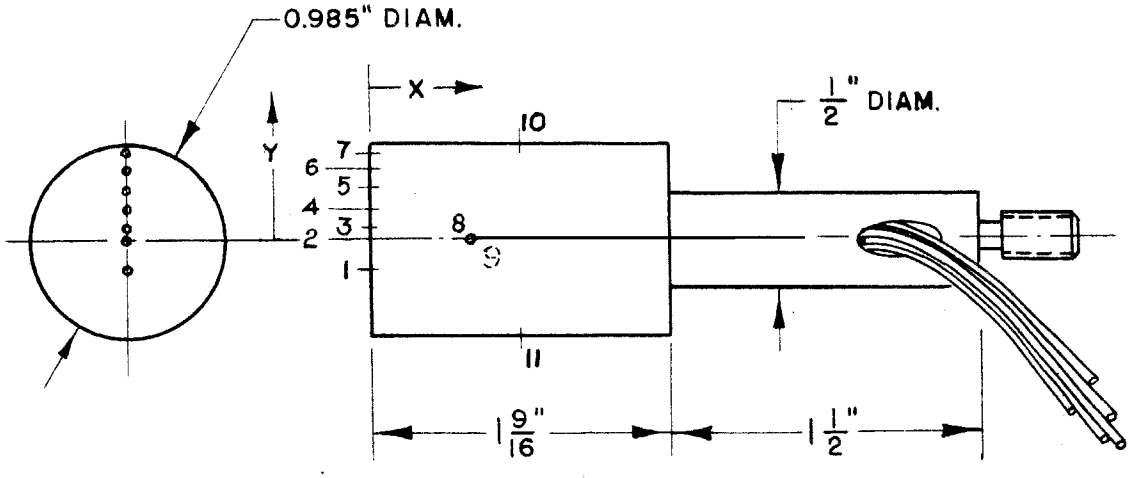

ORIFICE	X (IN.)	Y (IN.)
1	0	-.157
2	0	0
3	0	.055
4	0	.148
5	0	.244
6	0	.344
7	0	.446
8	.507	0
9	.517	0
10	.800	.492
11	.804	.492

CIRCULAR CYLINDER WITH ITS MAJOR AXIS PARALLEL TO THE FREE STREAM FLOW

FIGURE 17

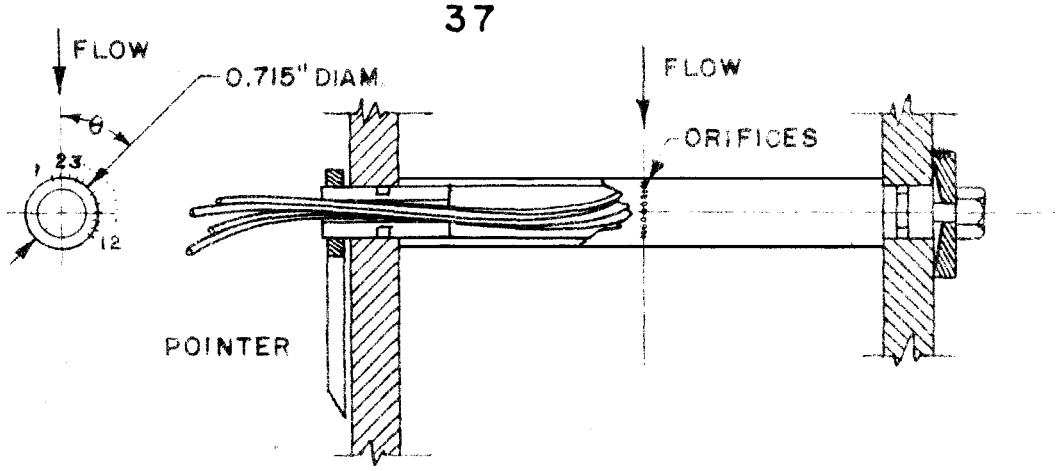

ORIFICE	1	2	3	4	5	6	7	8	9	10	11	12
θ (RAD.)	-.469	0	.219	.466	.686	.904	1.140	1.379	1.625	1.813	2.054	2.300

(A) STATIC PRESSURE MODEL

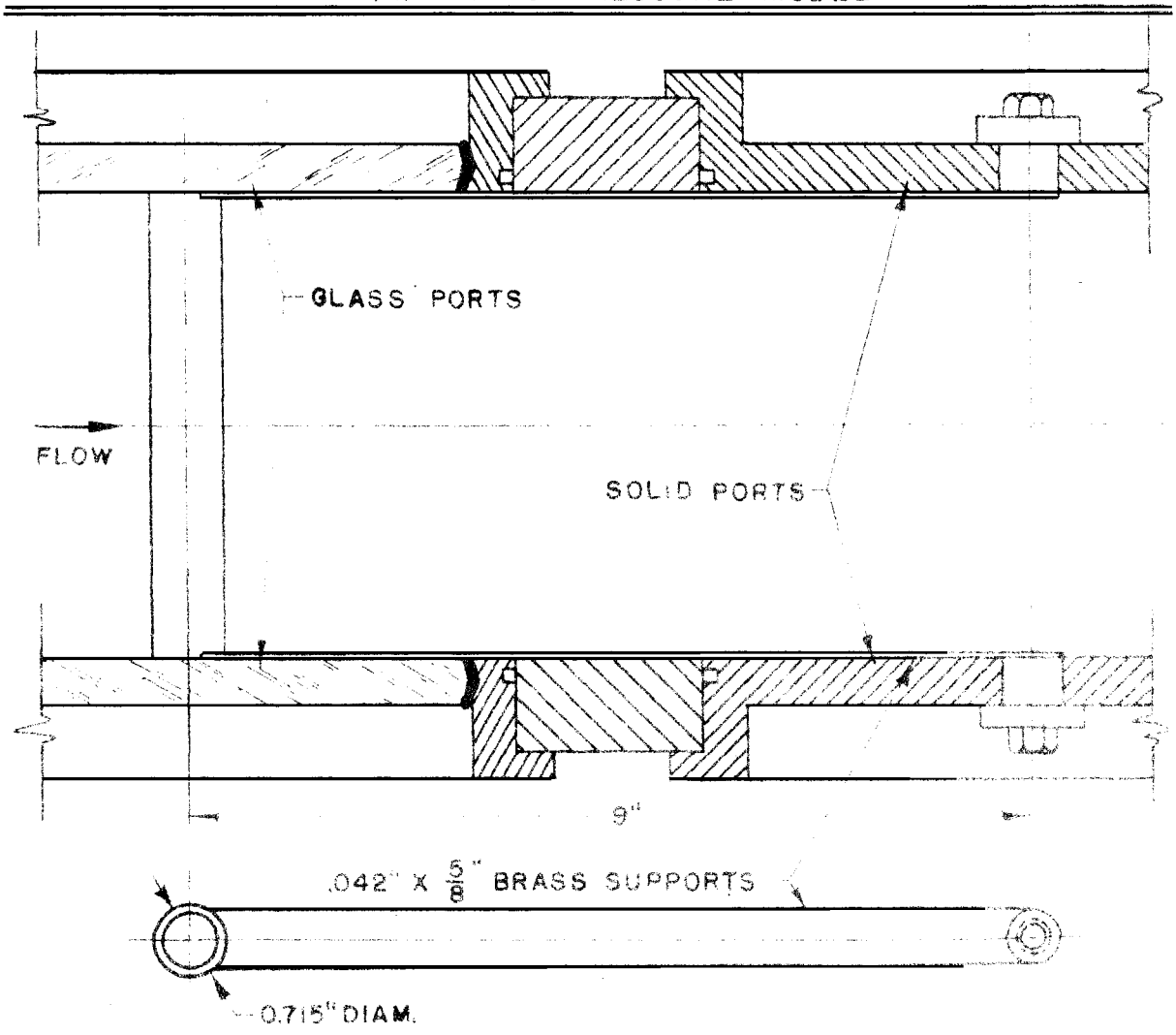

(B) SCHLIEREN MODEL

CIRCULAR CYLINDER TRANSVERSE TO FREE STREAM FLOW

FIGURE 18

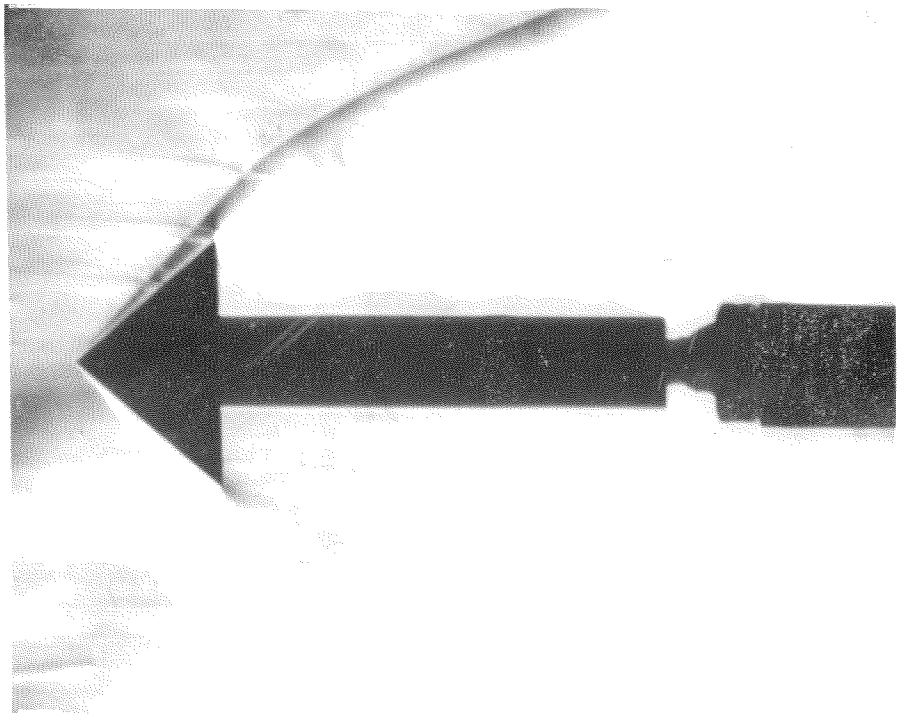

Schlieren Photograph of 40° Half-Angle Cone
$M_{\infty} = 5.8$
Figure 19

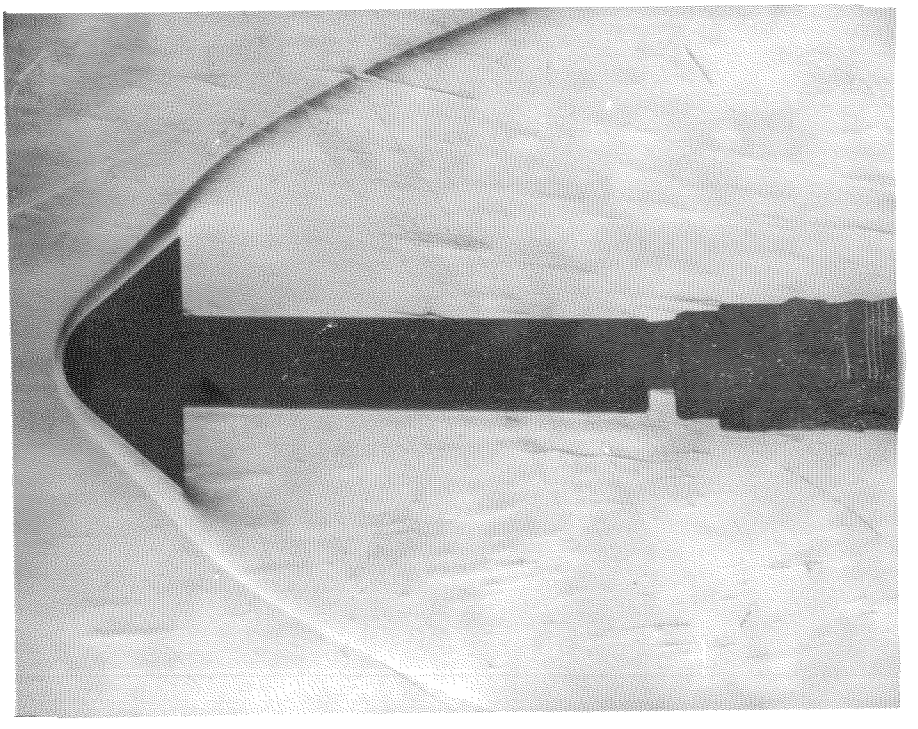

Schlieren Photograph of 40° Half-Angle Cone
with Spherical Nose - $M_{\infty} = 5.8$
Figure 20

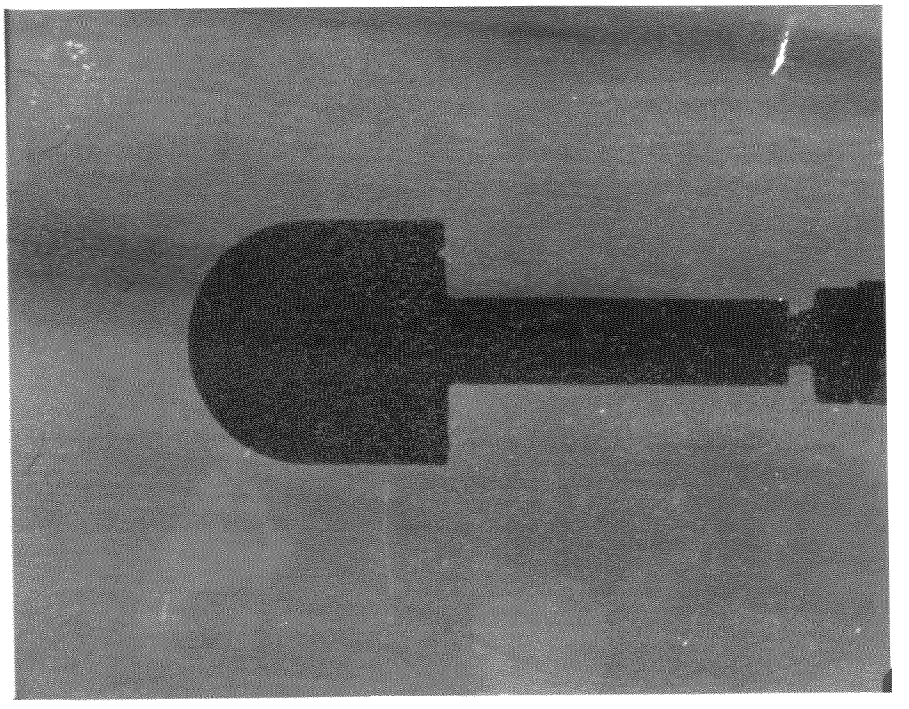

Schlieren Photograph of Hemisphere-Cylinder
$M_\infty = 5.8$
Figure 21

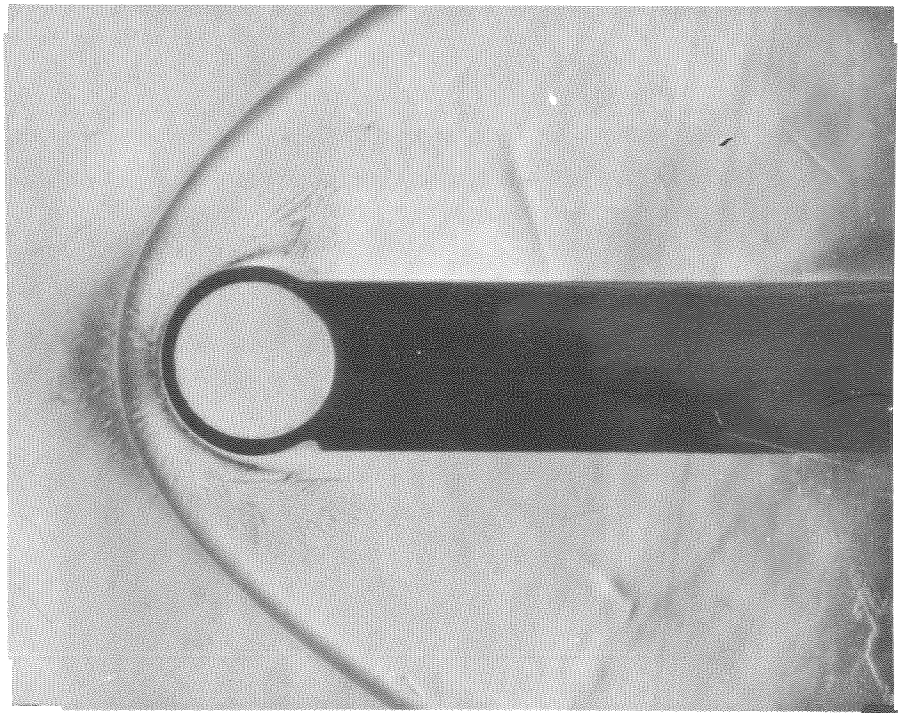

Schlieren Photograph of Circular Cylinder
Transverse to Free Stream Flow - $M_\infty = 5.8$
Figure 22

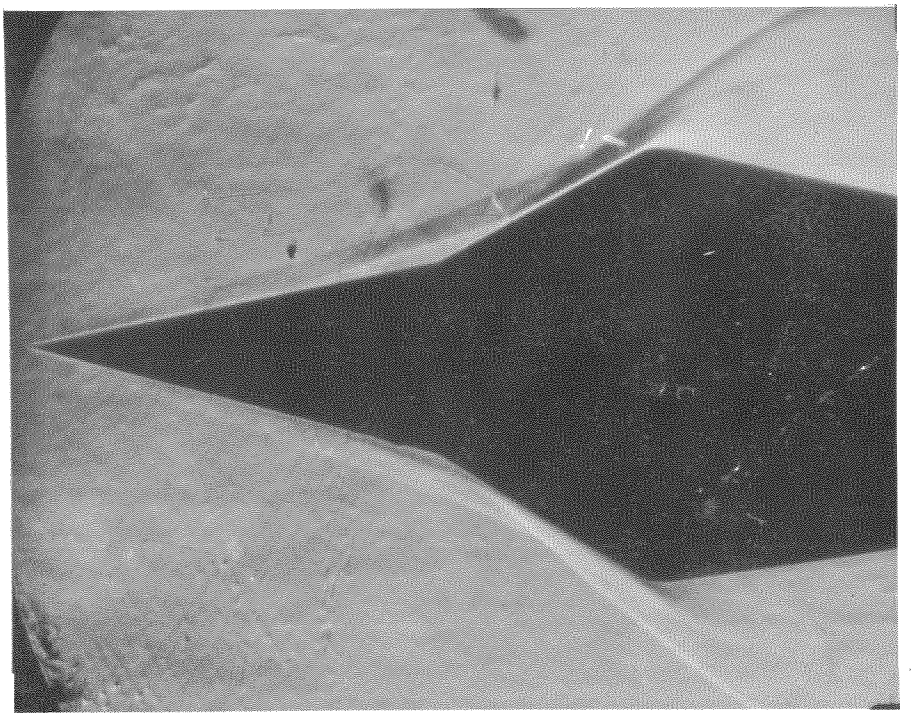

Schlieren Photograph of 13^{o} - 30^{o} Half-Angle Double Cone Re/In = 2.38×10^{5} $M_{\infty} = 5.8$
Figure 23

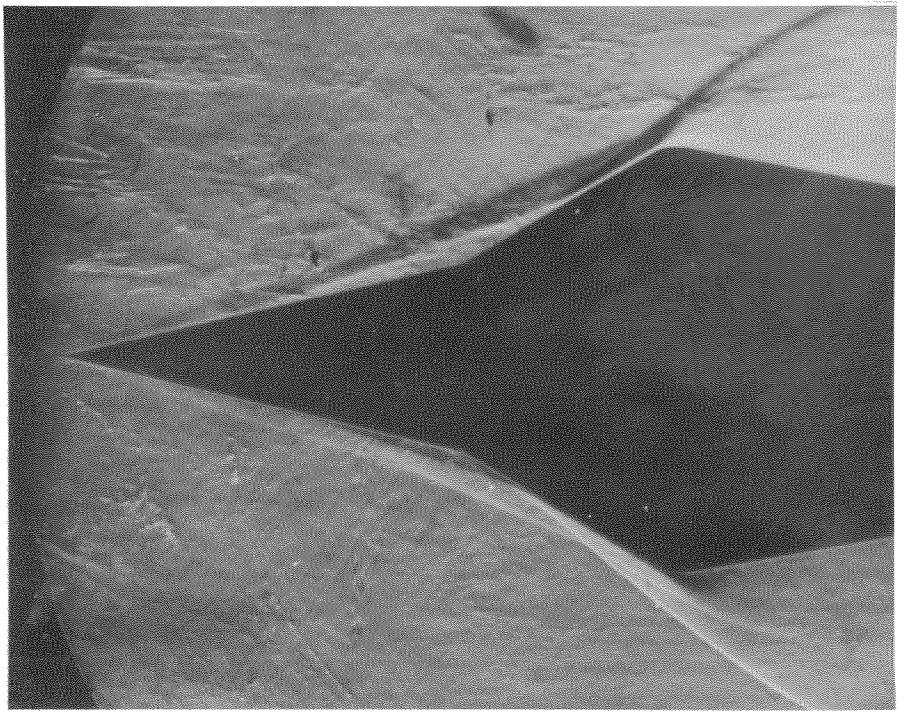

Schlieren Photograph of 13^{o} - 30^{o} Half-Angle Double Cone Re/In = 0.65×10^{5} $M_{\infty} = 5.6$
Figure 24

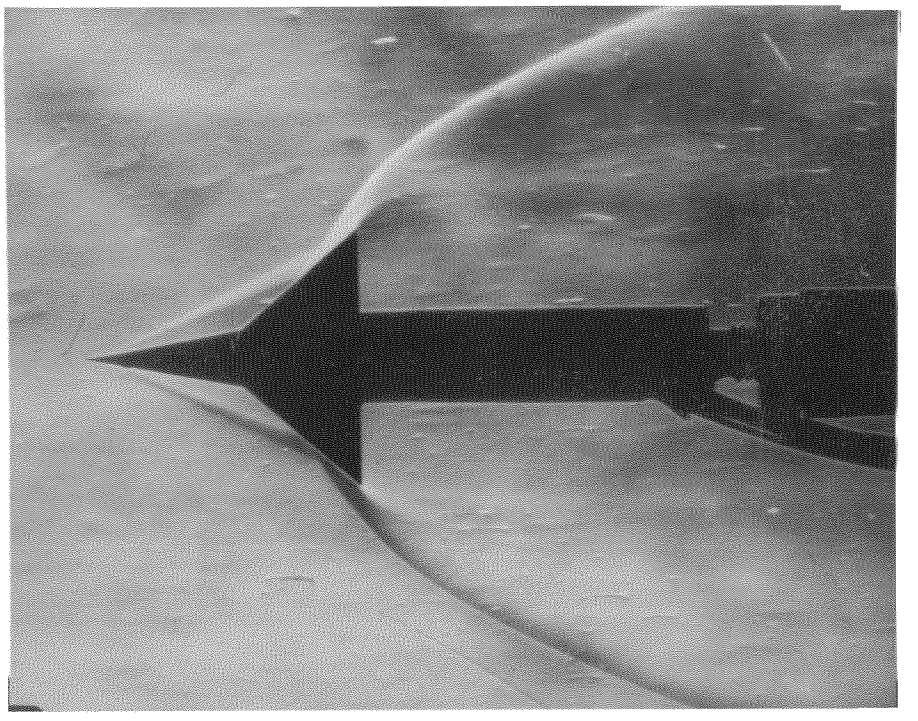

Schlieren Photograph of 10° - 40° Half-Angle
Double Cone - $M_{\infty} = 5.8$
Figure 25

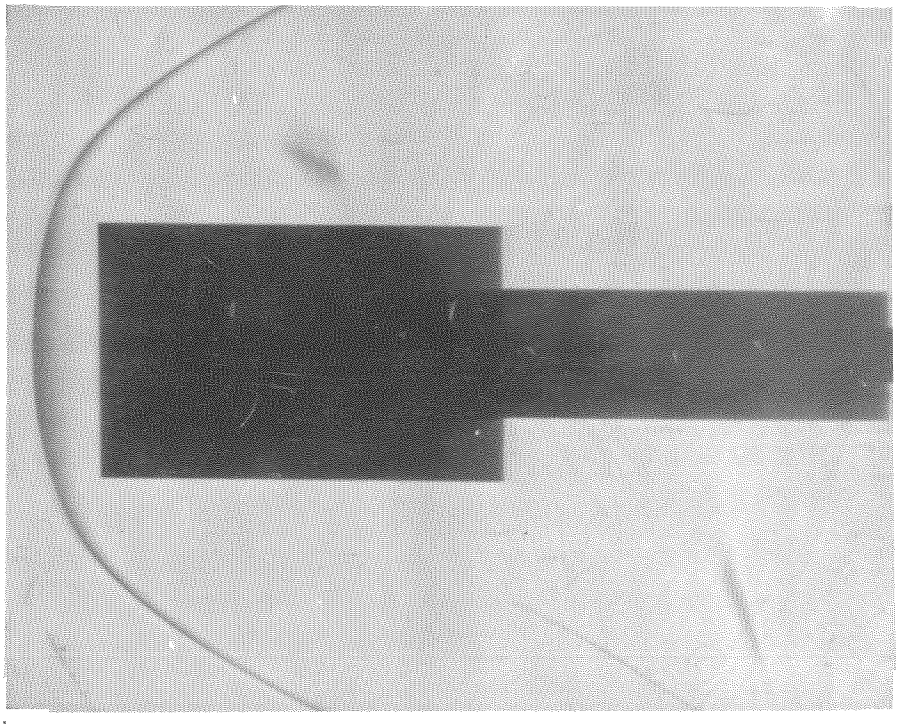

Schlieren Photograph of Flat-Nosed Cylinder
$M_{\infty} = 5.8$
Figure 26

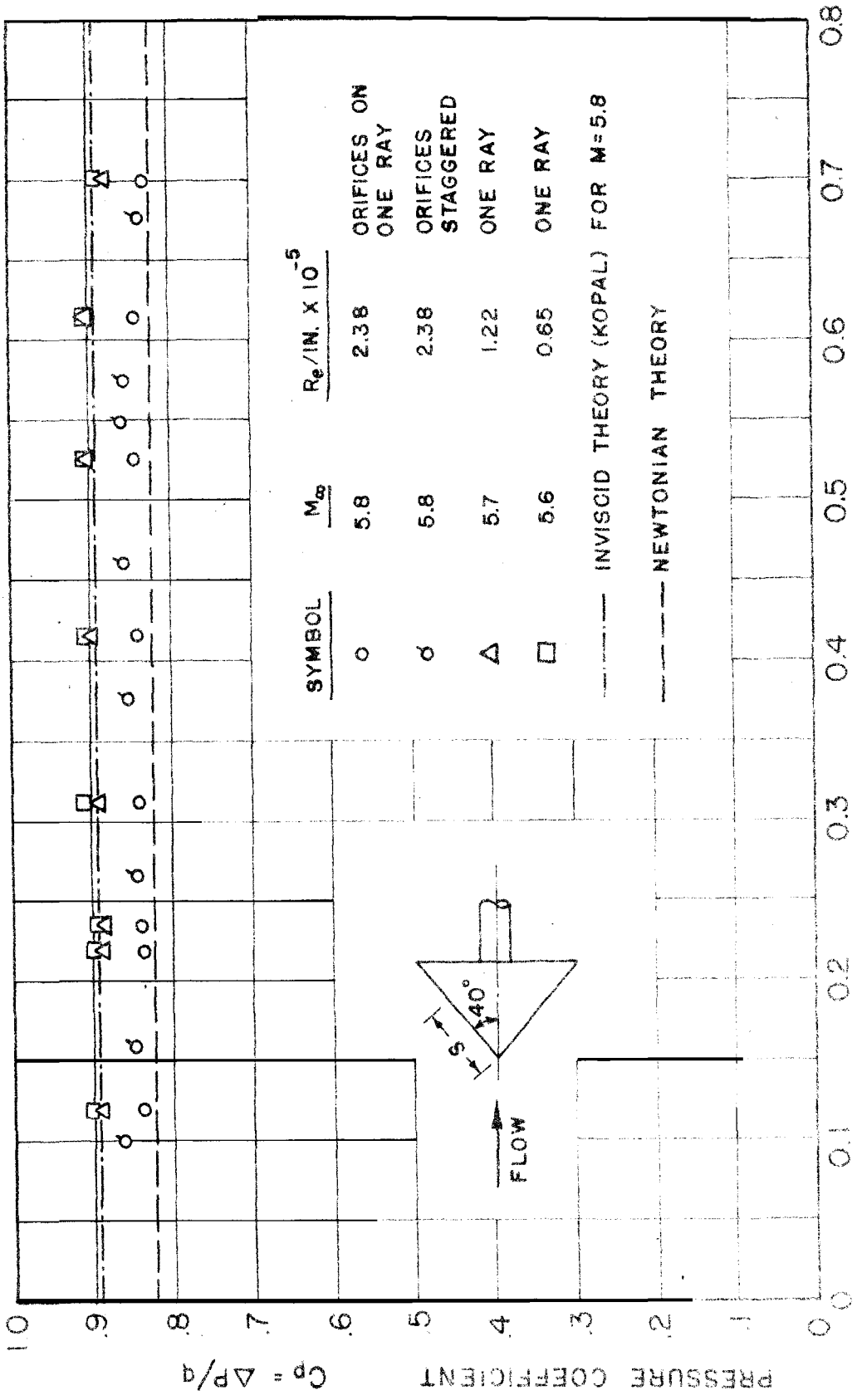

FIGURE 27

PRESSURE DISTRIBUTION ON THE SURFACE OF A 40° HALF-ANGLE CONE

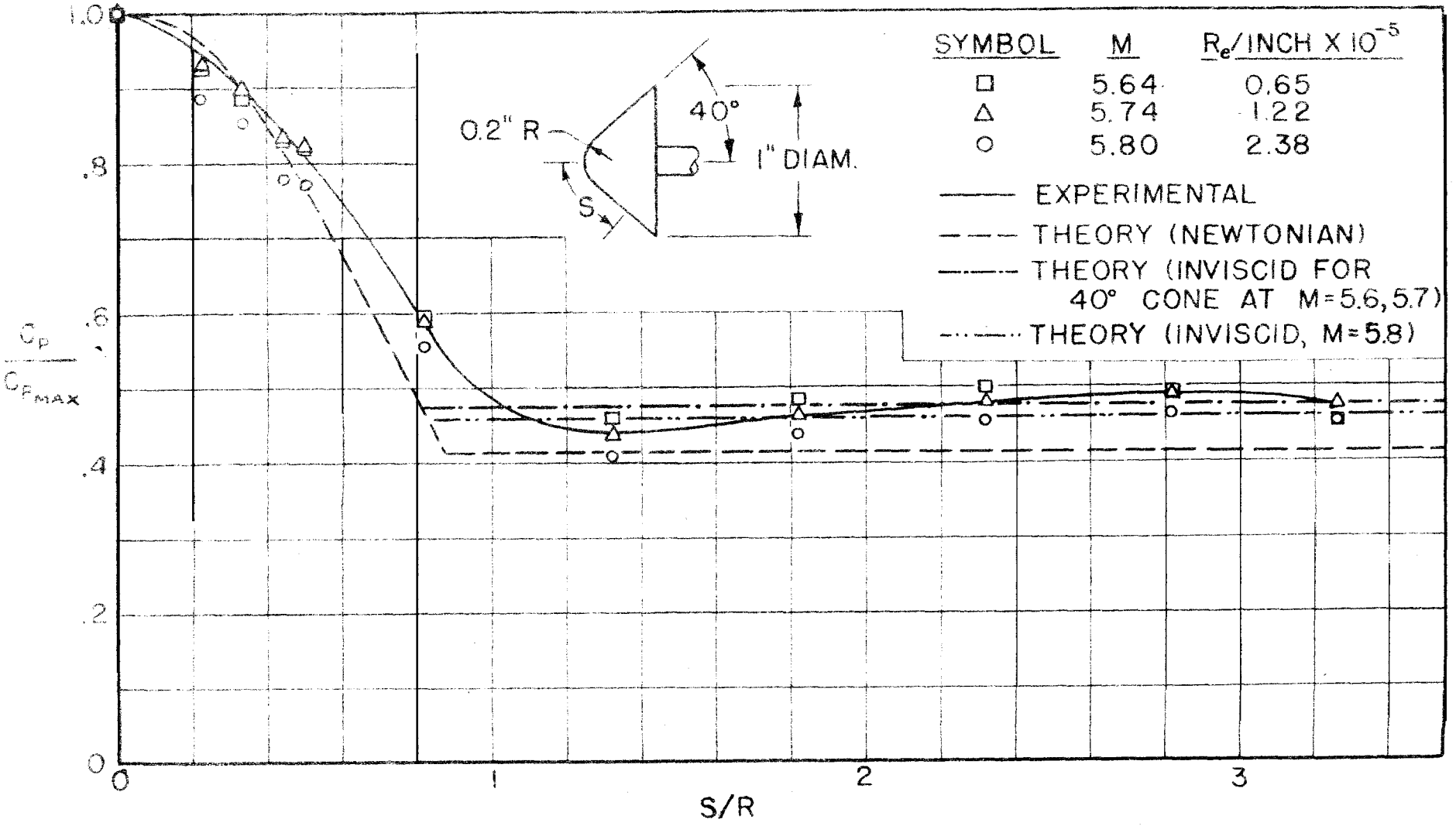

SURFACE PRESSURE DISTRIBUTION ON SPHERICAL NOSED CONE

FIG. 28

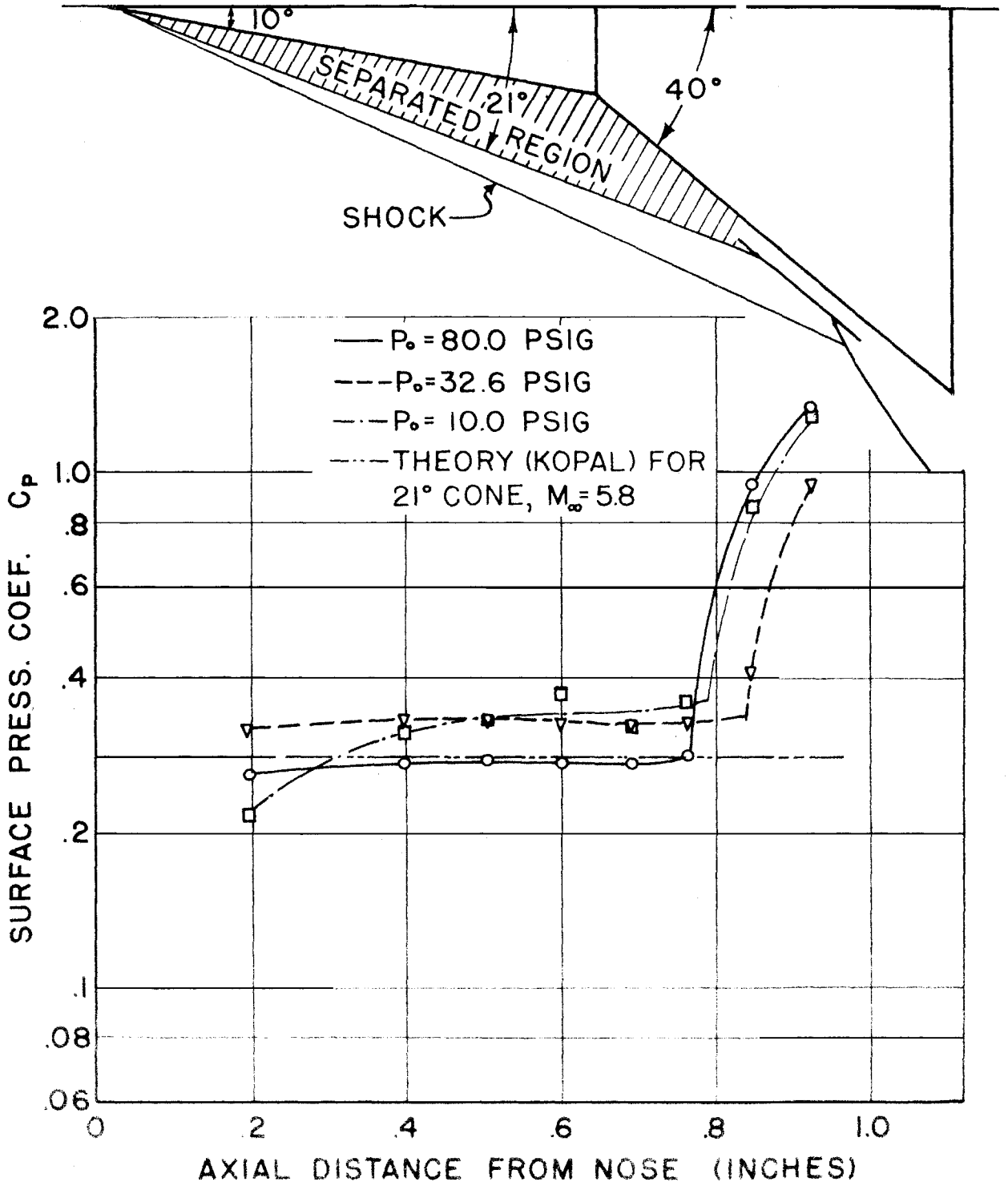

FIG. 29

PRESSURE DISTRIBUTION ON THE SURFACE OF A 10°-40° HALF ANGLE DOUBLE CONE

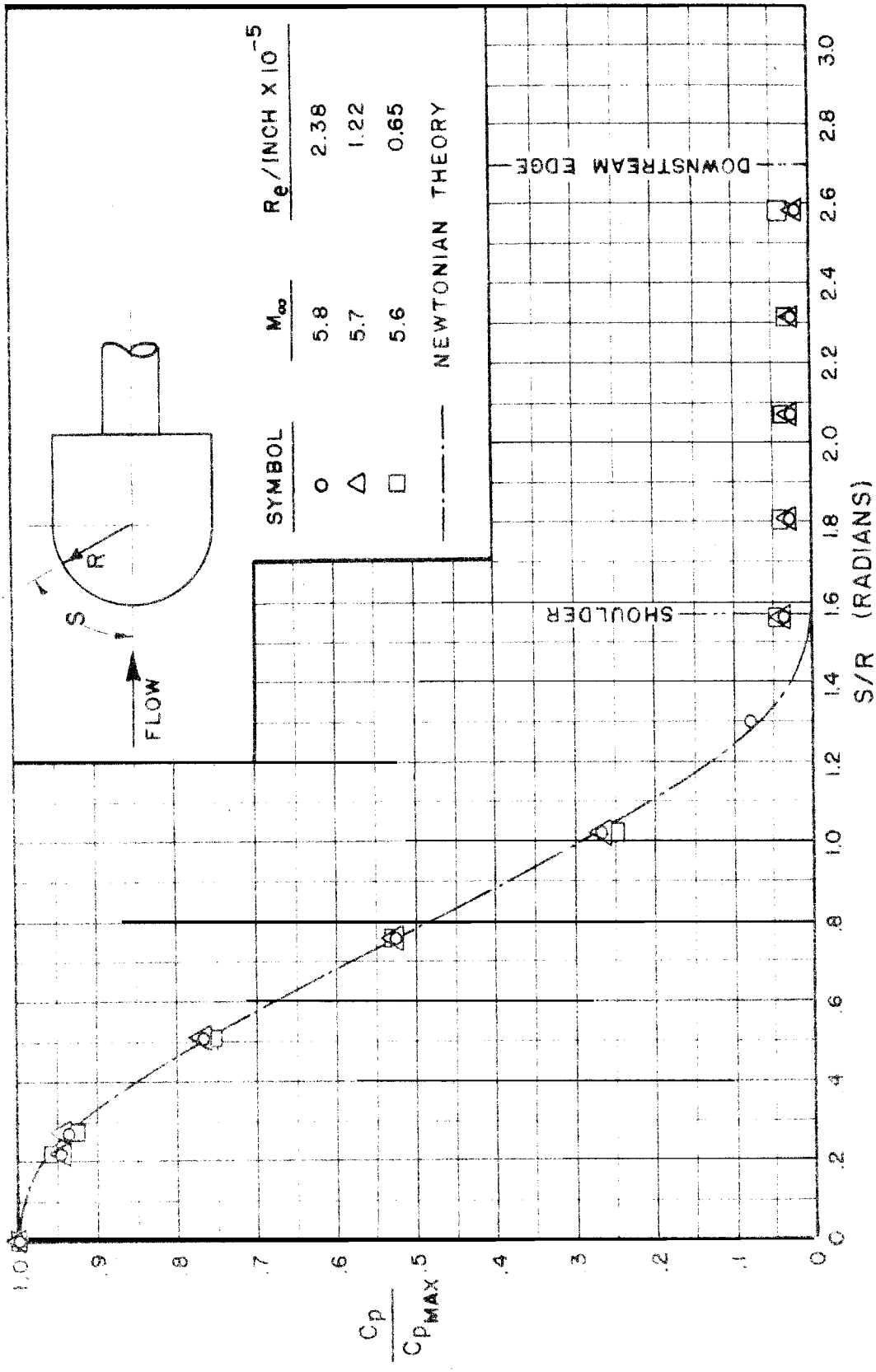

FIGURE 30

PRESSURE DISTRIBUTION ON THE SURFACE OF A HEMISPHERE-CYLINDER

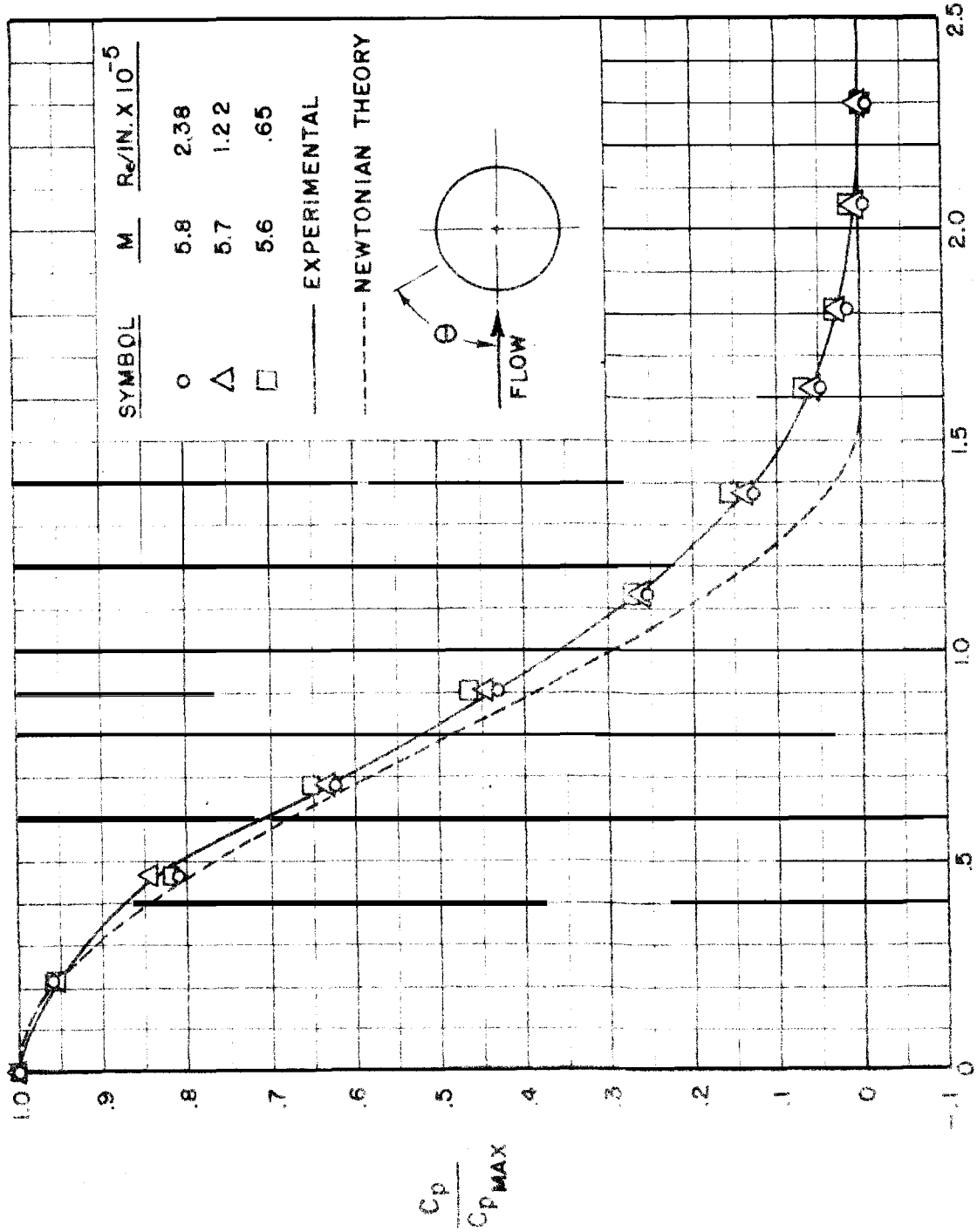

PRESSURE DISTRIBUTION ON A CIRCULAR CYLINDER TRANSVERSE TO FLOW

FIGURE 31

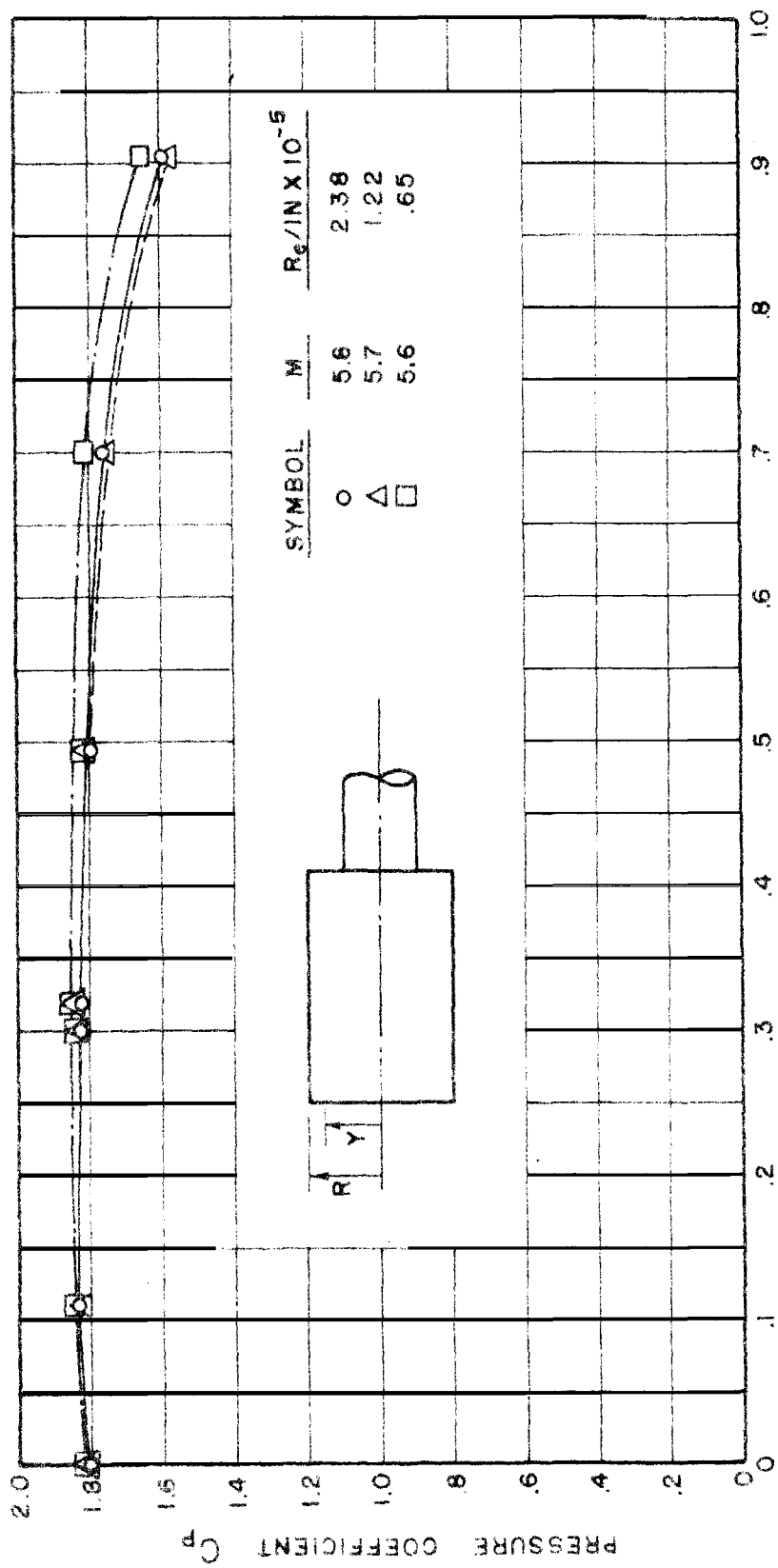

PRESSURE DISTRIBUTION ON THE FACE OF A FLAT NOSED CIRCULAR CYLINDER

FIGURE 32